BACHELORARBEIT

Cavity protection in Cavity QED with an inhomogeneous ensemble of emitters strongly coupled to a single cavity mode

ausgeführt am

Institut für Theoretische Physik
der Technischen Universität Wien

Institute for Theoretical Physics
Vienna University of Technology

unter der Anleitung von
Univ.Ass. Dr.rer.nat. Dmitry Krimer
und
Univ.Prof. Dipl.-Ing. Dr.techn. Stefan Rotter
durch

Benedikt Hartl
Czerningasse 14/17
A-1020 Wien
e1026773@student.tuwien.ac.at

August 18, 2013

_____
Datum

_____
Unterschrift

Contents

1. Introduction

The idea of resonantly coupling an ensemble of emitters with a single cavity mode was motivated in the early 1980s when Cavity Quantum Electrodynamics (CQED) was developed [1]. Experiments in this field rely on the fact that for the description of interaction between an electromagnetic field in the cavity and the ensemble of N two level systems (TLS), the whole ensemble can be treated as one effective spin variable, which behaves like a harmonic oscillator in the limit of low excitation energy [2]. Although a single spin is only slightly coupled to the cavity mode, the collective coupling of the ensemble is enhanced by the factor $\sqrt{N}$ [1, 3], allowing to reach the strong coupling regime requested for quantum information applications [4]. Thus when writing single excitations into the ensemble of N spins, the coupling between the cavity mode and the spin ensemble benefits from the collective interaction of all spins with the radiation field [3].

Different types of ensembles have been proposed such as clouds of ultra-cold atoms on a chip [5] or color centers in diamonds [6]. When such ensembles are strongly coupled to a cavity mode, they are considered as a promising physical realization for processing and storage of quantum information, provided that single excitations can coherently be written to and retrieved from the ensemble [2, 7].

The experimental setup studied in this thesis consists of a high-Q superconducting coplanar waveguide resonator (cavity) coupled to a diamond with negatively charged nitrogen-vacancy defects (NV-centers), which can be treated as an ensemble of bosonic spins [6, 8]. For such a setup the strong coupling regime has been observed in former studies [4, 8] proving that a NV-center diamond coupled to a high-Q cavity provides a promising approach towards a solid state quantum memory.

The ensemble of emitters consists of many individual bosonic spins with individual frequencies inhomogeneously distributed around a certain mean frequency [8, 9], which, in our considerations, is in resonance with the cavity mode frequency [10]. We modeled this inhomogeneously broadened spin ensemble (IHBSE) by a normalized, continuous spectral density distribution with full width at half maximum (FWHM) γ_q and mean frequency ω_s [9, 10]. With such an approach we end up with a rather complicated problem, because an excitation in the ensemble will be re-emitted into the cavity at a frequency with an individual weight given by the spectral density of the ensemble of the emitters. Thus the back-coupling to the cavity mode is partially suppressed because of the relative dephasing of the excitations due to the IHBSE [8].

In this thesis, we study the interaction of a single cavity mode strongly coupled to a continuous distribution of inhomogeneously broadened emitters in the low excitation regime at zero temperature. It should be noted that the relaxation properties of the undriven system initially prepared in an excitation depend both on the shape and on the width of the continuous spin distribution [9]. Even without cavity and spin losses, which describe the limiting lowest decay rate of the coupled cavity mode - spin ensemble without inhomogeneous broadening, we find a dephasing of an excitation in the system due to the presence of IHBSE [9]. In this work, we demonstrate under which conditions the influence of IHBSE on the decaying process can be significantly suppressed such that the decay rate reaches practically its minimal possible value given by the cavity and single spin losses rates (the so-called cavity protection regime). We consider here the realistic values for the collective coupling strengths Ω in contrast to [9], where this regime was demonstrated to exist under certain conditions as a limiting case only, in particular when Ω is much larger than the FWHM γ_q of the spin distribution. For this purpose we keep a finite Ω but modify the spin distribution in a specific way such that it supports the coherence properties of Rabi oscillations between the ground and excited state of the coupled system. Our goal is to achieve a reduced overlap of the two Rabi-states with other eigenstates of the Hamiltonian occurring due to the inhomogeneous bath of spins interacting with the cavity mode [9] and therefore reduce the decoherence of the observed Rabi-oscillations.

2. Model

The model under study consists of a cavity mode $a(t)$ with frequency ω_c and damping rate κ, coupled to a normalized distribution of N two-level systems (TLS) $\sigma_k(t)$ with individual frequency ω_k and damping rate γ [8] at zero temperature [10]. As we consider transmission through the cavity only in the case of a relatively weak field, only a small number of the N two-level systems compared to the ensemble size is excited [8]. Each two-level system can thus be modeled by a bosonic spin mode $\sigma_k^-(t)$ (Holstein-Primakoff approximation) [9], where $\sigma_k^-(t)$ is a Pauli spin-flip operator. The basic model for the interaction between a cavity mode and an ensemble of two-level systems is the Jaynes-Cummings model [11]. The cavity mode $a(t)$ is linearly coupled with a strength g_k to the individual spin and with a collective strength Ω to the ensemble. The spin ensemble consists of many individual bosonic spins $\sigma_k(t)$ with frequency ω_k distributed around a certain mean frequency ω_s and is modeled by a normalized, continuous spectral density distribution with full width at half maximum (FWHM) γ_q [8, 9]. In this thesis we considered ω_s to be in resonance with the cavity mode ω_c [10]. The strong coupling regime due to the collective coupling of the ensemble to the cavity mode can be observed as an avoided crossing in the transmission function of the cavity [5, 6, 8].

For preparing an excitation of the whole system, the cavity is pumped by a coherent microwave (probe-)field with (probe-)frequency ω_p and strength η [5]. A photon entering the cavity will be absorbed into an excitation of the ensemble spins. It will be re-emitted at a frequency with an individual weight given by the spectral density of the ensemble of the emitters. Thus the back-coupling to the cavity mode is partially suppressed because of the relative dephasing of the excitations due to the broad distribution of the spins [8].

In this thesis we test some methods which were predicted to enhance the coherence time of the Rabi oscillation between the coupled system of cavity mode $a(t)$ and the continuous distribution of bosonic spins $b_k(t)$. In particular we test the *cavity-protection* mechanism put forward by Diniz et al. in [9] and described in section (3). Following K. Sander et al. in [8] we approximate the composed system of cavity and spin ensemble with the Tavis-Cummings Hamiltonian and include the probe field of the cavity

$$
\begin{align}
H &= H_{cav} + H_{em} + H_{int} + H_p, \tag{1a}\\
H_{cav} &= \hbar\omega_c a^\dagger a, \tag{1b}\\
H_{em} &= \frac{\hbar}{2}\sum_k^N \omega_k \sigma_k^z, \tag{1c}\\
H_{int} &= i\hbar\sum_k^N \left(g_k \sigma_k^- a^\dagger - g_k^* \sigma_k^+ a\right), \tag{1d}\\
H_p &= -i\hbar\left(\eta a^\dagger e^{-i\omega_p t} - \eta^* a e^{i\omega_p t}\right). \tag{1e}
\end{align}
$$

H_{cav} and H_{em} describe the unperturbed energies of the cavity and the N ensemble spins with frequencies ω_c and ω_k, respectively. H_p is the probe-field Hamiltonian and η is the probe-field amplitude. a and $a^\dagger$ are the annihilation and creation operator for an excitation in the cavity mode. σ_k^z is the Pauli-z operator and σ_k^+ and σ_k^- are Pauli spin-flip operators for the k-th spin, respectively. We find the following commutation rules:

$$
[a, a^\dagger] = 1, \quad [\sigma_k^+, \sigma_j^-] = \delta_{kj}\sigma_k^z, \quad [\sigma_k^-, \sigma_j^z] = +2\delta_{kj}\sigma_k^-, \quad [\sigma_k^+, \sigma_j^z] = -2\delta_{kj}\sigma_k^+. \tag{2}
$$

For a, $a^\dagger$, σ_k^z and $\sigma_k^\pm$ we did not write the explicit time dependence for simplification but in the Heisenberg picture we are dealing with time dependent operators which are coupled to each other due to their interaction described by eqs. (1d,1e). To describe the time evolution of an arbitrary system-operator $A(t)$ we can use the Heisenberg equation of motion

$$
\dot{A} = \frac{i}{\hbar}[H, A]. \tag{3}
$$

We aim to derive equations which include an input and output mechanism between the cavity and a probe field, the coupling of the cavity mode with a bath of inhomogeneously broadened spins σ_k^- and damping. Therefore we have to add a Langevin term $\mathcal{L}$ to the Heisenberg equation which was done for instance in [12]. We set $\hbar = 1$ and arrive at Heisenberg equations with damping for the cavity-mode creation operator $a(t)$ and the Pauli spin flip operator $\sigma_k^-(t)$ (for zero temperature)

$$\dot{a}(t) = i[H, a(t)] - \kappa a(t), \quad \dot{\sigma}_k^-(t) = i[H, \sigma_k^-(t)] - \frac{\gamma}{2}\sigma_k^-(t). \quad (4)$$

Here κ and γ are the damping rate of the cavity-mode and of the individual spin, respectively. The damped Heisenberg equations of motion for the operators $a(t)$, $a^\dagger(t)$, $\sigma_k^\pm(t)$ and $\sigma_k^z(t)$, after transformation into the frame rotating with the probe frequency ω_p

$$a(t) = \tilde{a}(t)e^{-i\omega_p t}, \quad \sigma_k^-(t) = \tilde{\sigma}_k^-(t)e^{-i\omega_p t} \quad (5)$$

are as follows

$$\dot{\tilde{a}} = -(\kappa + i\Delta_c)\tilde{a} + \sum_k g_k\tilde{\sigma}_k^- - \eta, \quad (6a)$$

$$\dot{\tilde{a}}^\dagger = -(\kappa - i\Delta_c)\tilde{a}^\dagger + \sum_k g_k\tilde{\sigma}_k^+ - \eta^*, \quad (6b)$$

$$\dot{\tilde{\sigma}}_k^- = -(\frac{\gamma}{2} + i\Delta_k)\tilde{\sigma}_k^- + g_k\tilde{a}\sigma_k^z, \quad (6c)$$

$$\dot{\tilde{\sigma}}_k^+ = -(\frac{\gamma}{2} - i\Delta_k)\tilde{\sigma}_k^+ + g_k\tilde{a}^\dagger\sigma_k^z, \quad (6d)$$

$$\dot{\sigma}_k^z = -2g_k\left(a^\dagger\sigma_k^- + a\sigma_k^+\right) \quad (6e)$$

with $\Delta_k = \omega_k - \omega_p$ and $\Delta_c = \omega_c - \omega_p$ being the individual detuning (the individual frequency mismatch) of the k-th spin and the cavity mode with respect to the probe-field, respectively [10]. g_k is assumed to be real. Fig. (1) shows a schematic plot of the coupled cavity mode - spin ensemble system with cavity losses and input and output field.
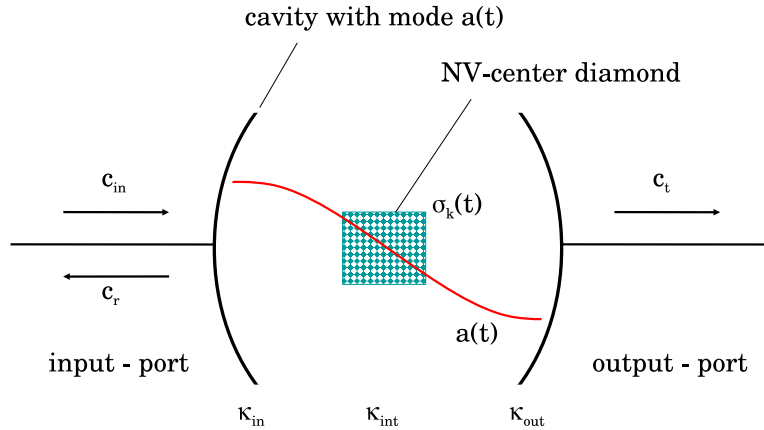

Figure (1) Schematic of the coupled cavity - spin ensemble system with Dirichlet boundary conditions for the cavity mode in the microwave resonator

2.1. Equation of motion for the expectation values

When we consider the weak-field limit of the probe-field and focus on low temperatures ($T \to 0\text{K}$) we can make the assumption that for the whole dynamics of the system only a small number of all spins in the ensemble is excited, so we fix

$$\langle \sigma_k^z(t) \rangle = -1 \tag{7}$$

similar to [8]. With this simplification we end up with a more simple set of coupled ODEs with respect to the cavity and spin amplitudes $a(t)$ and $\sigma_k^-(t)$. Taking the expectation values from eqs. (6a,6c) and using the well known input-output formalism for the cavity field described in [12] we get

$$\dot{A}(t) = -(\kappa + i\Delta_c)A(t) - \sqrt{2\kappa_{in}}\langle c_{in}(t)\rangle + \sum_k g_k B_k(t), \tag{8a}$$

$$\dot{B}_k(t) = -\left(\frac{\gamma}{2} + i\Delta_k\right)B_k(t) - g_k A(t), \tag{8b}$$

$$\langle c_r(t)\rangle = \langle c_{in}(t)\rangle + \sqrt{2\kappa_{in}}A(t), \tag{8c}$$

$$\langle c_t(t)\rangle = \sqrt{2\kappa_{out}}A(t). \tag{8d}$$

Here we introduced the convention $A(t) = \langle \tilde{a}(t) \rangle$ and $B_k(t) = \langle \tilde{\sigma}_k^-(t) \rangle$. The cavity loss rate $\kappa = \kappa_{in} + \kappa_{out} + \kappa_{int}$ consists of three contributions caused by the input/output mirrors and by some internal losses of which the rates are denoted as κ_{in}, κ_{out} and κ_{int}, respectively. The cavity is considered as symmetrical such that $\kappa_{in} = \kappa_{out}$ and $\kappa_{int} = 0$ [13]. The operators $c_{in}(t)$, $c_r(t)$ and $c_t(t)$ describe the input, reflected and transmitted fields, respectively and we wrote $\langle \eta \rangle = \sqrt{2\kappa_{in}}\langle c_{in} \rangle$ for the input field.

2.2. Inhomogeneous spin broadening

The ensemble of N two-level systems is modeled by an ensemble of bosonic spins being distributed around a certain mean frequency ω_s which is, in this model, considered in resonance with the cavity mode frequency ω_c. We follow [8, 9] and treat the spin-distribution as a normalized, continuous spectral density $\varrho(\omega)$ introducing the collective coupling strength Ω :

$$\varrho(\omega) = \frac{1}{\Omega^2}\sum_k g_k^2 \delta(\omega - \omega_k), \tag{9a}$$

$$\int d\omega \varrho(\omega) = 1, \tag{9b}$$

$$\Omega^2 = \sum_k g_k^2. \tag{9c}$$

Previous works showed, that the best choice for the modal distribution for the spectral density is a q-Gaussian distribution [8, 10], defined as

$$\varrho(\omega) = N \cdot \left[1 - (1-q)\frac{(\omega - \omega_s)^2}{\Delta^2}\right]^{\frac{1}{1-q}} \tag{10}$$

with q and γ_q listed in tbl. (1). $\gamma_q = 2\Delta\sqrt{\dfrac{2^q - 2}{2q - 2}}$ is the FWHM and N is a normalization factor which is obtained numerically from the normalization condition (9b) [8].

2.3. Solutions of the Volterra integral equation

The steady-state solution $A_{st}(t)$ for the cavity-mode is derived by setting $\dot{A}(t) = 0$ in eq. (8a) and $\dot{B}_k(t) = 0$ in eq. (8b) and then inserting $B_k(t)$ from eq. (8b) into eq. (8a). Next we use

the property of $\varrho(\omega)$ which allows us to pass from a discrete sum $\sum_k g_k^2 F(\omega_k)$ to a continuous expression $\Omega^2 \int d\omega \varrho(\omega) F(\omega)$ in frequency, so we find

$$A_{st}(t) = \frac{i\sqrt{2\kappa_{in}}\langle c_{in}\rangle}{\omega_c - \omega_p - i\kappa - \Omega^2 \int d\omega \dfrac{\varrho(\omega)}{\omega - \omega_p - i\dfrac{\gamma}{2}}}. \tag{11}$$

This will become the non-trivial initial condition $A_{st}(t) = A(0)$ for the dynamics of the cavity mode $A(t)$ when the probe field is switched off at time $t = 0$.

Using the definition for the transmission: $T(\omega_p) = \langle c_t\rangle / \langle c_{in}\rangle$ and inserting eq. (11) into eq. (8d), the transmission function in the steady state regime for different probe field frequencies ω_p becomes

$$T(\omega_p) = \frac{2i\sqrt{\kappa_{out}\kappa_{in}}}{\omega_c - \omega_p - i\kappa + W(\omega_p)}, \tag{12}$$

with

$$W(\omega_p) = \Omega^2 \int d\omega \frac{\varrho(\omega)}{\omega_p - \omega + i\dfrac{\gamma}{2}}. \tag{13}$$

The following derivation was done by D. Krimer in [10] where we can see a good agreement of theory and experiment for the decay of the undriven system initially prepared in the steady state regime. Here we just summarize the results. When the system sets into the steady-state-regime the input-field is switched off at $t = 0$ and eqs.(8a-8d) modify, as we consider $\omega_p = 0$, with the notation introduced above as follows:

$$\dot{A}(t) = -(\kappa + i\omega_c)\,A(t) + \sum_k g_k B_k(t), \tag{14a}$$

$$\dot{B}_k(t) = -(\gamma/2 + i\omega_k)\,B_k(t) - g_k A(t). \tag{14b}$$

Now we transform into (a kind of) rotating frame with frequency ω_c and damping rate κ

$$A(t) = \tilde{A}(t)e^{-i(\omega_c - i\kappa)t} \tag{15}$$

and derive the Volterra integral equation from eqs. (14a-14b) with $A(0) = \tilde{A}(0)$ given by eq. (11):

$$\tilde{A}(t) = \int_0^t d\tau \mathcal{K}(t - \tau)\tilde{A}(\tau) + \mathcal{F}(t). \tag{16}$$

It contains the kernel function $\mathcal{K}(t - \tau)$

$$\mathcal{K}(t - \tau) = \Omega^2 \int d\omega \frac{\varrho(\omega)\left[e^{-i(\omega - \omega_c - i(\gamma/2 - \kappa))(t - \tau)} - 1\right]}{i(\omega - \omega_c - i(\gamma/2 - \kappa))}, \tag{17}$$

and the function $\mathcal{F}(t)$ which appears due to the nontrivial initial conditions

$$\mathcal{F}(t) = \tilde{A}(0)\left\{1 + \Omega^2 \int d\omega \frac{\varrho(\omega)\left[1 - e^{-i(\omega - \omega_c - i(\gamma/2 - \kappa))t}\right]}{(\omega - \omega_p - i\gamma/2)(\omega - \omega_c - i(\gamma/2 - \kappa))}\right\}. \tag{18}$$

The integral equation eq. (16) for $\tilde{A}(t)$ consists of an integral over the product of $\mathcal{K}(t - \tau)$ and $\tilde{A}(\tau)$ from $\tau = 0$ to $\tau = t$ and an additional function $\mathcal{F}(t)$, which appears due to the nontrivial initial conditions. We see that $\tilde{A}(t)$ depends on all former solutions of $\tilde{A}(\tau)$ with $\tau < t$, but also on the value of $\tilde{A}(\tau = t)$ and thus the cavity mode $A(t)$ given by eq. (15) is a nontrivial quantity. The integration is basically performed numerically by applying the trapezoid formula on eq. (16). For more details on the derivation of the numerical solution of the Volterra integral equation, see appendix.

2.4. Reference results without cavity protection

To make contact with previous calculations in [10] figure (2) shows the spectral density of the spin ensemble $\varrho(\omega)$ (a), the absolute value squared of the transmission function $|T(\omega_p)|^2$ in the steady-state regime (b) and the time evolution of an excitation in the cavity mode $|\langle a(t) \rangle|^2$ for the resonance condition $\omega_s = \omega_c = \omega_p$ (c) with effective coupling strength $\Omega/2\pi = 10$MHz and parameters listed in table (1). The axes of ((a),(b),(c)) are scaled to the same spacing as figures (4,5,6) to simplify comparison.
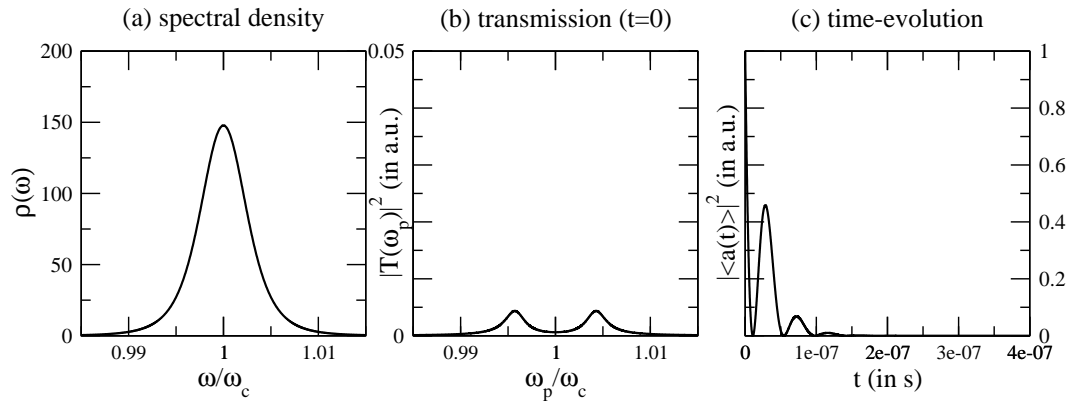

Figure (2)   Reference plot without cavity protection (a) $\varrho(\omega)$ defined in eq. (10) (q-Gaussian) versus normalized frequency ω, (b) absolute value squared of the transmission function in the steady-state regime $|T(\omega_p)|^2$ defined in eq. (12) versus normalized probe frequency ω_p, (c) time evolution of an excitation in the cavity mode $|\langle a(t) \rangle|^2$ defined in eq. (16) for the resonance condition $\omega_s = \omega_c = \omega_p$ versus time, with effective coupling strength $\Omega/2\pi = 10$MHz and parameters summarized in tbl. (1).

2.5. Parameters

Here some parameters are listed, which we used in our calculations. They describe the coupled cavity mode - spin ensemble system and are taken from [10].

Parameter	Value
$\omega_c/2\pi$	2.6919 GHz
$\omega_s/2\pi$	2.6919 GHz
q	1.389
$\gamma_q/2\pi$	15.5 MHz
$\kappa_{in}/2\pi$	0.2 MHz
$\kappa_{out}/2\pi$	0.2 MHz
$\kappa_{int}/2\pi$	0 MHz
$\gamma/2\pi$	1.6 MHz
q_{cp}	1.5
β	$1.9 \cdot 10^4$
$\Delta\omega$	$0.05 * \Delta_{cp}$
$\Delta\varrho$	$\frac{1}{e}\varrho(\omega_s \pm \Omega)$

Table (1)   Parameters used in the calculations

3. Basic idea of cavity protection

As was mentioned in the beginning of this report Diniz et al. proposed in [9], that for small γ_q/Ω the full width at half maximum (FWHM) of the two peaks of the absolute value squared of the transmission function $T(\omega_p)$ defined by eq. (12) and shown in fig. (2b) becomes

$$\Gamma = \kappa + \gamma/2 + \pi\varrho\left(\omega_s \pm \Omega\right) \cdot \Omega^2. \tag{19}$$

Γ should become independent of the inhomogeneous broadening of $\varrho(\omega)$ defined by eq. (10) and shown in fig. (2a) and should only depend on the losses of the cavity and of individual emitters, respectively, if one increases the ratio Ω/γ_q, provided $\varrho(\omega)$ decays faster than $1/\omega^2$. We call this effect *cavity protection*. The contribution of the inhomogeneous broadening of the spin spectrum with FWHM γ_q to the width Γ writes $\pi\varrho\left(\omega_s \pm \Omega\right) \cdot \Omega^2$. For a rectangular spin distribution for instance $\pi\varrho\left(\omega_s \pm \Omega\right) \cdot \Omega^2$ becomes zero for a finite Ω where for a Gaussian distribution this remains a limit and for a Lorentzian distributions it is a constant value [9]. We see that the shape of $\varrho(\omega)$ has a dramatic influence on the behavior of the system.

3.1. Derivation of the decay rate of the undriven excited system

In this section we will set the cavity mode frequency ω_c as the reference frequency. Starting from our expression for the transmission function eq. (12) we first take care of $W(\omega_p)$ defined by eq. (13). Following the derivation of Diniz et al. in [9] in Appendix C we find for $W(\omega_p)$ by expansion

$$
\begin{aligned}
W(\omega_p) &= \Omega^2 \int\limits_{-\infty}^{\infty} d\omega \frac{\varrho(\omega)}{\omega_p - \omega + i\gamma/2} \cdot \frac{\omega_p - \omega - i\gamma/2}{\omega_p - \omega - i\gamma/2} \\
&= -\Omega^2 \int\limits_{-\infty}^{\infty} d\omega' \frac{\omega'^2}{\omega'^2 + \gamma'^2} \frac{\varrho(\omega_p + \omega')}{\omega'} - i\pi\Omega^2 \int\limits_{-\infty}^{\infty} d\omega' \frac{\gamma'}{\pi\left[\omega'^2 + \gamma'^2\right]} \varrho(\omega_p + \omega')
\end{aligned}
\tag{20}
$$

where we used $\gamma' = \gamma/2$ for simplification and substituted $\omega' = \omega - \omega_p$ to find eq. (C1) from Diniz (except for the wrong sign in their first integral which doesn't matter later on when we substitute back). We can identify each of the integrands as a product of a function of width γ' and $\varrho(\omega)$ defined in eq. (10) with FWHM γ_q. When we keep a finite but small $\gamma' \ll \gamma_q$ (which is correct for the situation we want to describe [10], compare table (1)) we can expand $\frac{\omega'^2}{\omega'^2 + \gamma'^2}$ and $\frac{\gamma'}{\pi\left[\omega'^2 + \gamma'^2\right]}$ in terms of γ'. For the first expression we simply write

$$\frac{\omega'^2}{\omega'^2 + \gamma'^2} \approx 1, \tag{21}$$

but for the second expression we have to be careful about the expansion with respect to γ', because in the limit $\gamma' = 0$ we can identify

$$
\begin{aligned}
\lim_{\gamma' \to 0} \frac{\gamma'}{\pi\left[\omega'^2 + \gamma'^2\right]} &= \lim_{\gamma' \to 0} \frac{\left(\frac{1}{\gamma'}\right)}{\pi\left[1 + \left(\frac{1}{\gamma'^2}\right)\omega'^2\right]} = \lim_{n \to \infty} \frac{n}{\pi\left[1 + n^2\omega'^2\right]} \\
&= \delta(\omega'),
\end{aligned}
\tag{22}
$$

which is a representation of a delta distribution. By expansion of $\frac{\gamma'}{\pi\left[\omega'^2 + \gamma'^2\right]}$ to the linear term we find

$$
\begin{aligned}
\frac{\gamma'}{\pi\left[\omega'^2 + \gamma'^2\right]} &\approx \left.\frac{\gamma'}{\pi\left[\omega'^2 + \gamma'^2\right]}\right|_{\gamma'=0} + \left.\left(\frac{1}{\pi\left[\omega'^2 + \gamma'^2\right]} + \frac{\gamma'}{\pi\left[\omega'^2 + \gamma'^2\right]^2}(-2\gamma')\right)\right|_{\gamma'=0} \cdot \gamma' \\
&\approx \delta(\omega') + \frac{1}{\pi\omega'^2}\gamma',
\end{aligned}
\tag{23}
$$

where we have to avoid the second summand in the linear term of the expansion at the frequency $\omega' = 0$ to find the results of Diniz et al. in [9]. We suppose, this can be done, because we are only interested in the variation of the delta distribution due to a finite γ' and the second summand would only be another delta distribution. We have to be careful again especially in the vicinity of $\omega' = 0$, when we insert eqs. (22-23) into eq. (20). $W(\omega_p)$ then becomes

$$W(\omega_p) = \Omega^2 \cdot \mathcal{P} \int_{-\infty}^{\infty} d\omega \frac{\varrho(\omega)}{\omega_p - \omega} - i\Omega^2 \left\{ \pi\varrho(\omega_p) + \frac{\gamma}{2} \cdot \mathcal{P} \int_{-\infty}^{\infty} d\omega \frac{\varrho(\omega)}{(\omega_p - \omega)^2} \right\}, \qquad (24)$$

which again agrees with [9] (C2). We substituted $\omega = \omega_p + \omega'$. $\mathcal{P}$ stands for principal value. Further we are interested in the behavior of $W(\omega_p)$ near the maxima of the transmission function ($\omega_p \approx \pm\Omega$) so we rewrite eq. (24) with $\frac{\omega}{\omega_p} = r$ as follows

$$\begin{aligned} W(\omega_p) &= \frac{\Omega^2}{\omega_p} \cdot \mathcal{P} \int_{-\infty}^{\infty} d\omega \frac{\varrho(\omega)}{1 - \frac{\omega}{\omega_p}} - i\Omega^2 \left\{ \pi\varrho(\omega_p) + \frac{\gamma}{2\omega_p{}^2} \cdot \mathcal{P} \int_{-\infty}^{\infty} d\omega \frac{\varrho(\omega)}{(1 - \frac{\omega}{\omega_p})^2} \right\} \\ &= \frac{\Omega^2}{\omega_p} \cdot \mathcal{P} \int_{-\infty}^{\infty} d\omega \frac{\varrho(\omega)}{1 - r} - i\Omega^2 \left\{ \pi\varrho(\omega_p) + \frac{\gamma}{2\omega_p{}^2} \cdot \mathcal{P} \int_{-\infty}^{\infty} d\omega \frac{\varrho(\omega)}{(1 - r)^2} \right\}. \end{aligned} \qquad (25)$$

For $r < 1$ (or $\omega < \omega_p$) we can rewrite $\frac{1}{1-r} = \sum_{k=0}^{\infty} r^k$ and $\left(\frac{1}{1-r}\right)^2 = \sum_{l=0}^{\infty} r^l \cdot \sum_{m=0}^{\infty} r^m = \sum_{k=0}^{\infty} (k+1)r^k$ and we find for

$$\begin{aligned} W(\omega_p) = & \frac{\Omega^2}{\omega_p} \cdot \mathcal{P} \int_{-\infty}^{\infty} d\omega \sum_{k=0}^{\infty} \left(\frac{\omega}{\omega_p}\right)^k \varrho(\omega) \\ & - i\Omega^2 \left\{ \pi\varrho(\omega_p) + \frac{\gamma}{2\omega_p{}^2} \cdot \mathcal{P} \int_{-\infty}^{\infty} d\omega \sum_{k=0}^{\infty} (k+1) \left(\frac{\omega}{\omega_p}\right)^k \varrho(\omega) \right\}. \end{aligned} \qquad (26)$$

By defining the k-th moment of $\varrho(\omega)$ around its origin

$$\mu_k = \int_{-\infty}^{\infty} d\omega \varrho(\omega) \omega^k, \qquad (27)$$

we find by reordering integral and sum

$$W(\omega_p) = \frac{\Omega^2}{\omega_p} \left\{ 1 + \sum_{k=1}^{\infty} \frac{\mu_k}{\omega_p^k} \right\} - i\Omega^2 \pi\varrho(\omega_p) - i\frac{\Omega^2}{\omega_p^2} \frac{\gamma}{2} \left\{ 1 + \sum_{k=1}^{\infty} (k+1) \frac{\mu_k}{\omega_p^k} \right\}, \qquad (28)$$

which agrees with Diniz (C3), except for the term $-i\Omega^2 \pi\varrho(\omega_p)$ which they misleadingly put into the first curly brackets and so multiplied $-i\Omega^2 \pi\varrho(\omega_p)$ by $1/\omega_p$. Diniz (C5) is correct again for this term.

Note that the derivation only holds for $r = \frac{\omega}{\omega_p} < 1$ which has to be treated carefully. In eq. (24) we integrate from $-\infty$ to $+\infty$ over all frequencies ω, so we can't write $\int_{-\infty}^{\infty} d\omega \frac{1}{1 - \frac{\omega}{\omega_p}} \varrho(\omega) = \int_{-\infty}^{\infty} d\omega \sum_{k=0}^{\infty} (\frac{\omega}{\omega_p})^k \varrho(\omega)$ unless we make some further simplifications. When we consider the limit $\Omega \gg \gamma_q$ and by only looking at the vicinity of the poles $\omega_p \approx \pm\Omega$ of

the transmission function, we can modify the boundaries of the integral: $-\infty \to \omega_{min}$ and $\infty \to \omega_{max}$ with $\omega_{max} - \omega_s \ll \Omega$ and $\varrho(\omega_{min}) = \varrho(\omega_{max}) \approx 0$. Thus we can write

$$\int_{-\infty}^{\infty} d\omega \frac{1}{1 - \frac{\omega}{\omega_p}} \varrho(\omega) \approx \int_{-\omega_{min}}^{\omega_{max}} d\omega \sum_{k=0}^{\infty} (\frac{\omega}{\omega_p})^k \varrho(\omega) = \sum_{k=0}^{\infty} \frac{\mu_k}{\omega_p^k}. \tag{29}$$

We consider the limit $\gamma \ll \gamma_q \ll \Omega$ and expect the poles of the transmission function to be located around $\omega_p \approx \pm\Omega$. We can identify $\mu_0 = 1$, $\mu_1 = 0$ (due to the symmetric function $\varrho(\omega)$) and $\mu_2 \neq 0$ as first non-vanishing moment (which is typically proportional to the square of the FWHM of $\varrho(\omega)$ as Diniz stated in [9]). Finally with $\frac{\Omega^2}{\omega_p + i\gamma/2} \approx \frac{\Omega^2}{\omega_p} - i\frac{\Omega^2}{\omega_p^2}\frac{\gamma}{2}$ we can write

$$\begin{aligned} W(\omega_p) &\approx \frac{\Omega^2}{\omega_p} \left\{ 1 + \frac{\mu_2}{\omega_p^2} \right\} - i\Omega^2\pi\varrho(\omega_p) - i\frac{\Omega^2}{\omega_p^2}\frac{\gamma}{2} \left\{ 1 + 3\frac{\mu_2}{\omega_p^2} \right\} \\ &\approx \frac{\Omega^2}{\omega_p + i\gamma/2} \left\{ 1 + \frac{\mu_2}{\omega_p^2} \right\} - i\Omega^2\pi\varrho(\omega_p), \end{aligned} \tag{30}$$

which agrees with [9] (C5) but doesn't hold for [6, 8, 10] where we find similar parameters like those listed in tbl. (1). We are dealing with a situation where $\Omega \approx 2\pi \cdot 10\text{MHz}$ is of the same magnitude as γ_q. We thus have to significantly modify either γ_q or Ω or, as we did in this report, $\varrho(\omega)$.

Never the less we are looking for the complex poles of the transmission function defined by eq. (12) by inserting $W(\omega_p)$ from eq. (30)

$$T(\omega_p) \approx \frac{-2i\sqrt{\kappa_{out}\kappa_{in}}}{\omega_p + i\kappa - \frac{\Omega^2}{\omega_p + i\gamma/2} \left\{ 1 + \frac{\mu_2}{\omega_p^2} \right\} + i\Omega^2\pi\varrho(\omega_p)}, \tag{31}$$

where we set the denominator equal to zero

$$\omega_p + i\kappa - \frac{\Omega^2}{\omega_p + i\gamma/2} \left\{ 1 + \frac{\mu_2}{\omega_p^2} \right\} + i\Omega^2\pi\varrho(\omega_p) = 0. \tag{32}$$

This equation can't be solved analytically for an arbitrary spin distribution, so we have to make some further simplifications. We expect the peaks of $T(\omega_p)$ to remain located around $\omega_p \approx \pm\Omega$ so we set $\varrho(\omega_p \approx \Omega) = const$ as we consider $\gamma \ll \gamma_q \ll \Omega$. We further said that $\mu_2 \propto \gamma_q^2 \ll \Omega^2$ which leads us to the conclusion that $\frac{\mu_2}{\omega_p^2} \approx \frac{\mu_2}{\Omega^2} = const$ and so eq. (32) simplifies to

$$\omega_p + i\kappa - \frac{\Omega^2}{\omega_p + i\gamma/2} \left\{ 1 + \frac{\mu_2}{\Omega^2} \right\} - i\Omega^2\pi\varrho(\Omega) = 0. \tag{33}$$

Now we easily find the complex poles

$$\omega_p^{(\pm)} = -i\frac{1}{2} \left[\kappa + \pi\Omega^2\varrho(\Omega) + \gamma/2 \right] \pm \Omega\sqrt{1 + \frac{\mu_2}{\Omega^2} - \frac{1}{4\Omega^2} \left[\kappa + \pi\Omega^2\varrho(\Omega) - \gamma/2 \right]^2}. \tag{34}$$

We can interpret the real part of $\omega_p^{(\pm)}$ as the position of the peaks of the transmission function on the real ω-axis. The imaginary part $\Gamma_A = \frac{1}{2}[\kappa + \pi\Omega^2\varrho(\Omega) + \gamma/2]$ describes the damping rate of the amplitudes and we identify the damping rate $\Gamma = \kappa + \pi\Omega^2\varrho(\Omega) + \gamma/2$ for the absolute value squared of the transmission function, which agrees with eq. (19).

3.2. Limiting decay rate

In this section we determine the lowest decay rate which can be achieved, if the inhomogeneous broadening of $\varrho(\omega)$ has no influence on the dynamics of the system

$$\Gamma_{\text{limit}} = \kappa + \gamma/2 = \kappa_{in} + \kappa_{out} + \kappa_{int} + \gamma/2. \tag{35}$$
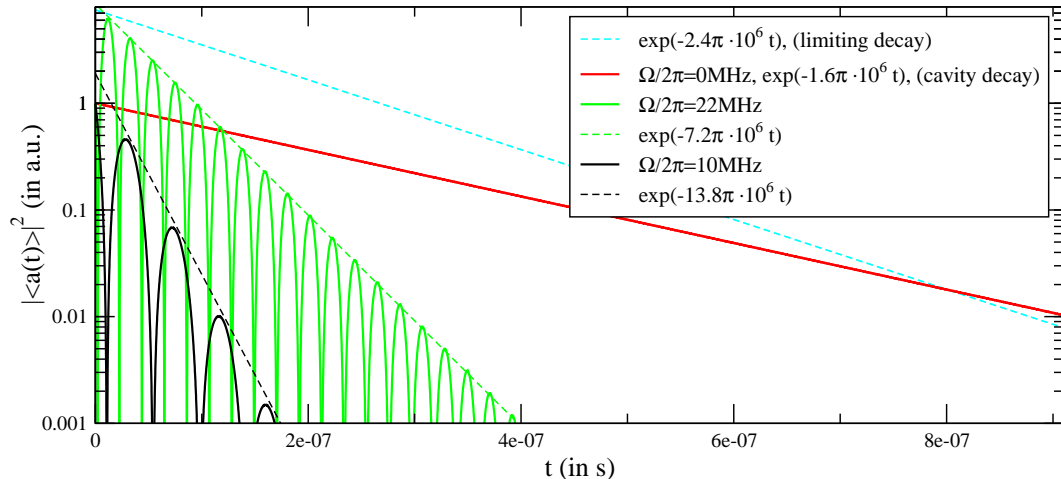
Figure (3) Comparing limiting decay eq. (36) (cyan dashed line) with the time evolution of an excitation in the cavity mode $|\langle a(t) \rangle|^2$ defined in eq. (16) for the resonance condition $\omega_s = \omega_c = \omega_p$ with no coupling $\Omega = 0$MHz (red curve), with effective coupling strength $\Omega = 2\pi \cdot 10$MHz (black curve) and $\Omega = 2\pi \cdot 22$MHz (green curve). The black and green dashed lines denote the effective decay for the time evolution of $|\langle a(t) \rangle|^2$ with $\Omega = 2\pi \cdot 10$MHz and $\Omega = 2\pi \cdot 22$MHz, respectively. Parameters are summarized in tbl. (1).

This limit is called the cavity protection regime. With the parameters summarized in table (1) we find a limiting decay rate of $\Gamma_{\text{limit}}/2\pi = (0.2 + 0.2 + 0 + 1.6/2)MHz= 1.2$MHz. By combining eq. (11), eq. (12) and eq. (8d) we find, that $|T(\omega_p)|^2$ is proportional to $|A_{st}(t)|^2$ and thus we can identify eq. (35) as limiting decay rate for the time evolution of the cavity mode and the limiting decay becomes

$$|A(t)|^2_{\text{limit}} \propto e^{-\Gamma_{\text{limit}}t}. \tag{36}$$

Another limiting case for the decay rate is zero coupling, which means that every $g_k = 0$ and thus $\Omega = 0$. In this limit $\tilde{A}(t)$ in eq. (16) is a constant value $\tilde{A}(0)$ and by taking the absolute value squared of eq. (15)

$$|A(t)|^2_{\Omega=0} = |\tilde{A}(0)|^2 e^{-2\kappa t} \tag{37}$$

we find an exponential decay of the excitation in the cavity mode with a rate $2\kappa/2\pi = 0.8$MHz (see table (1)).

Figure (3) compares the limiting decay eq. (36) (cyan dashed line), the limit of no coupling $\Omega = 0$MHz given by eq. (37) (red line) and the time evolution of an excitation in the cavity mode $|\langle a(t) \rangle|^2$ defined in eq. (16) for the resonance condition $\omega_s = \omega_c = \omega_p$ with effective coupling strength $\Omega = 2\pi \cdot 10$MHz (black curve) and $\Omega = 2\pi \cdot 22$MHz (green curve). The black and green dashed lines denote the effective decay for the time evolution of $|\langle a(t) \rangle|^2$ with $\Omega = 2\pi \cdot 10$MHz and $\Omega = 2\pi \cdot 22$MHz, respectively.

Here we see, that for increasing Ω we indeed find an enhanced lifetime of the Rabi oscillation but we are still not in the limit $\Omega \gg \gamma_q$. For $\Omega \gg \gamma_q$ the q-Gaussian spin distribution we used in this thesis effectively looks like a delta function.

3.3. Cavity protection by an effective continuous spin distribution

We found that the contribution of the inhomogeneously broadened spin distribution to the decay rate Γ defined by eq. (19) depends on the value of the spectral density of the emitters at the frequency $\omega_s \pm \Omega$. Γ should therefore become independent of the width γ_q when

one removes a small interval of the spectrum of the spins in the vicinity of the frequencies $\omega_{cp}^{(\pm)} = \omega_s \pm (\Omega + \delta\Omega)$, respectively, so they can't couple to the cavity mode $a(t)$ anymore. The rest of the distribution remains untouched. $\delta\Omega$ is a small variation of the position of the dips. We define an effective spin distribution with two dips around $\omega_{cp}^{(\pm)}$ with dip-width Δ_{cp}, respectively,

$$\varrho_{\mathrm{eff}}(\omega) = \begin{cases} 0, \text{ for } \omega = \omega_{cp}^{(\pm)} \pm \Delta_{cp}/2 \\ \varrho(\omega), \text{ otherwise} \end{cases}, \tag{38}$$

and $\varrho(\omega)$ defined by eq. (9a). The subscript cp stands for cavity protection. We calculate the effective spin distribution by subtracting a cavity protection distribution $\varrho_{cp}(\omega)$ from the original distribution $\varrho(\omega)$ defined by eq. (10). This will generate two dips in the original distribution in the vicinity of the frequencies $\omega_{cp}^{(\pm)}$ which satisfy conditions specified in the appendix by eqs. (43). We further have to avoid negative values of the effective spin distribution in our calculations, which could appear due to the subtraction of $\varrho_{cp}(\omega)$

$$\varrho_{\mathrm{eff}}(\omega) = \begin{cases} \varrho(\omega) - \varrho_{\mathrm{cp}}(\omega), \text{ for } \varrho(\omega) \geq \varrho_{cp}(\omega) \\ 0, \text{ otherwise} \end{cases}. \tag{39}$$

As the subtraction of $\varrho_{cp}(\omega)$ describes a real loss of spins which couple to the cavity mode (but lead to decoherence) in the intervals $\omega_{cp}^{(\pm)} \pm \frac{1}{2}\Delta_{cp}$, $\varrho_{\mathrm{eff}}(\omega)$ is not normalized anymore. The new distribution describes an effective coupling with collective coupling strength $\Omega_{\mathrm{eff}} < \Omega$ because $\int d\omega \varrho_{\mathrm{eff}}(\omega) < 1$. This will alternate the time-evolution of the system as the period of the Rabi-oscillation is proportional to $1/\Omega_{\mathrm{eff}}$ [11].

Although we reduce the collective coupling strength we expect an enhanced lifetime and a reduced decay rate of the time evolution of the system. We aim to achieve a suppressed coupling of the dressed ground state $\left|\Psi_-^0\right\rangle = 1/\sqrt{2} \cdot (\left|1, G\right\rangle - i\left|0, S\right\rangle)$, which corresponds to the frequency $\omega_s - \Omega$, and the dressed excited state $\left|\Psi_+^0\right\rangle = 1/\sqrt{2} \cdot (\left|1, G\right\rangle + i\left|0, S\right\rangle)$, corresponding to $\omega_s + \Omega$ with the continuum of eigenstates of the Hamiltonian $\left|\Psi_\omega\right\rangle$. $\left|1, G\right\rangle$ denotes an excitation in the cavity mode $\left|1\right\rangle$ and the spin ensemble in the ground state $\left|G\right\rangle = \left|g, g, \cdots, g\right\rangle$. $\left|0, S\right\rangle$ describes no excitation in the cavity mode $\left|0\right\rangle$ and the first excited symmetric matter state $\left|S\right\rangle = 1/\sqrt{N} \cdot (\left|e, g, \cdots, g\right\rangle + \cdots + \left|g, \cdots, e, \cdots, g\right\rangle + \cdots + \left|g, \cdots, g, e\right\rangle)$, [5]. Without inhomogeneous broadening of the spin distribution, $\left|\Psi_\pm^0\right\rangle$ are not coupled to the continuum of (dark-)states $\left|\Psi_\omega\right\rangle$. With inhomogeneous broadening there is an overlap of the dressed states $\left|\Psi_\pm^0\right\rangle$ with the continuum of eigenstates $\left|\Psi_\omega\right\rangle$, respectively, as described in [9].

With the cavity protection mechanism explained above, we should decrease the width Γ of the two peaks of the absolute value squared of the transmission function, respectively, and thus reduce the overlap of the Rabi states with other eigenstates. This mechanism should provide an energy preservation in the dynamics of the system as the exchange of energy will now mostly happen between $\left|\Psi_-^0\right\rangle$ and $\left|\Psi_+^0\right\rangle$ in form of Rabi oscillation.

To be more insensitive with respect to the position $\omega_{cp}^{(\pm)}$ of the dips and the shape of $\varrho_{\mathrm{eff}}(\omega)$ in the calculation of the transmission function $T(\omega_p)$ and the time evolution $\langle a(t)\rangle$, respectively, we introduce three different shapes for the cavity protection distribution: the *rectangular distribution* denoted as $\varrho_{cp}^{(\mathrm{rec})}(\omega)$ and specified in the appendix by eq. (45), a more narrow *q-Gaussian distribution* denoted as $\varrho_{cp}^{(\mathrm{q})}(\omega)$ also specified in the appendix by eq. (47) and a more rectangular *Fermi-Dirac like distribution* denoted as $\varrho_{cp}^{(\mathrm{fd})}(\omega)$ specified by eq. (48) in the appendix.

We believe, that one can experimentally realize a proper $\varrho_{\mathrm{eff}}(\omega)$ by pumping a narrow band of the spectral density of the emitters into permanent excitation by irradiating the NV-Center diamond with a laser of frequency $\omega_{cp}^{(\pm)} \approx \omega_s \pm \Omega$, respectively. When all spins are excited in the ranges $\omega_{cp}^{(\pm)} \pm \Delta_{cp}/2$, respectively, we effectively burned two holes into the continuous spin distribution and the laser should be turned off to minimize thermal excitation. By doing so, we prepare the diamond in a proper way such that the modified

inhomogeneous spin ensemble should provide the minimal decay rate in a subsequent experiment. Since all spins in the ranges $\omega_{cp}^{(\pm)} \pm \Delta_{cp}/2$ are, then, considered to be excited, the cavity can't pump these spins into excitation anymore, hence it can't couple to them, as long as they remain excited. Photons may however originate from these spins irradiated with the laser and leak into the cavity, which may lead to a coupling again, when the experimental timescale is too long. In the next section, we use a stationary effective spin distribution and demonstrate theoretically a significantly reduced decay rate of the initially excited system without going to the limit $\Omega \gg \gamma_q$. Stationary means, that we consider the effective spin distribution as time independent.

4. Results of calculations

In the previous section we derived an expression for an effective spin distribution to check the cavity protection mechanism described above. Following D. Krimer's report [10] we start from his solutions of the Volterra integral equation (16) but with modified effective spin distributions for the emitters $\varrho_{\text{eff}}^{(\text{rec,q,fd})}(\omega)$ defined by eq. (38) and in the appendix. Our goal is to prove, if we can reach the limiting decay rate given by eq. (35) without going to the limit $\Omega \gg \gamma_q$, which Diniz et al. claimed in [9].

4.1. Different effective spin distributions

In this section we generate different effective spin distributions for our three shapes (rec, q, fd) with three values for the width of the dips $\Delta_{cp}^{(1,2,3)}$, respectively. The dips are located at the frequencies $\omega_{cp}^{(\pm)} = \omega_s \pm \Omega$ with the original coupling strength Ω but not at $\omega_{\text{eff}}^{(\pm)} = \omega_s \pm \Omega_{\text{eff}}$.

Fig. (4) shows the three different forms of $\varrho_{\text{eff}}^{(\text{rec,q,fd})}(\omega)$ (rectangular, q-Gaussian and Fermi-Dirac like) for three different width $\Delta_{cp}^{(1,2,3)}/2\pi = (1.3, 3.9, 6.5)$MHz for $\varrho_{cp}^{(\text{rec,q,fd})}(\omega)$ defined in the appendix. Other parameters are listed in tbl. (1), $\Omega = 2\pi \cdot 10$MHz and $\delta\Omega = 0$, respectively. As $\Delta_{cp}^{(i)}$ with $i = 1, 2, 3...$ defines the characteristic width of the dips (for more details, see appendix), we define the width $\Delta_{cp}^{(\text{xi})}$, used in the expressions for the cavity protection distributions defined in the appendix for the shape (x) = (rec, q, fd). Note that for $\varrho_{\text{eff}}^{(\text{rec})}(\omega)$ the effective distribution becomes 0 on both intervals $[\omega_{cp}^{(\pm)} - \frac{1}{2}\Delta_{cp}, \omega_{cp}^{(\pm)} + \frac{1}{2}\Delta_{cp}]$, respectively. For $\varrho_{\text{eff}}^{(\text{q})}(\omega)$ with characteristic width $\Delta_{cp}^{(1)}/2\pi = 1.3$ MHz there is just a narrow interval on both sides of ω_c (or actually two single points at $\omega_{cp}^{(\pm)}$) where $\varrho_{\text{eff}}^{(\text{q})} = 0$, respectively. The Fermi-Dirac like distribution $\varrho_{\text{eff}}^{(\text{fd})}(\omega)$ describes a bit broader intervals $[\approx (\omega_{cp}^{(-)} - \frac{1}{2}\Delta_{cp}^{(\text{fd})}), \omega_{cp}^{(-)}]$ and $[\omega_{cp}^{(+)}, \approx (\omega_{cp}^{(+)} + \frac{1}{2}\Delta_{cp}^{(\text{fd})})]$ where $\varrho_{\text{eff}}^{(\text{fd})}(\omega) = 0$, respectively and one may define a $\delta\Omega \approx -\frac{1}{4}\Delta_{cp}^{(\text{fd})}$ to ensure $\varrho_{\text{eff}}^{(\text{fd})}(\omega)$ becomes zero on an interval around $\omega_{cp}^{(\pm)}$.

4.2. Effective steady-state regime due to cavity protection

When we use eq. (12) for the transmission function and replace $\varrho(\omega)$ shown in fig. (2a) with $\varrho_{\text{eff}}(\omega)$, we expect the transmission $|T(\omega_p)|^2$ around $\omega_{cp}^{(\pm)}$ to get higher so the peaks should grow and their width should become smaller.

Figure (5) shows the absolute value squared of the transmission function $|T(\omega_p)|^2$ in the steady-state regime for different shapes of the effective distribution $\varrho_{\text{eff}}^{(\text{rec,q,fd})}(\omega)$ arranged in columns and widths $\Delta_{cp}^{(1,2,3)}/2\pi = (1.3, 3.9, 6.5)$MHz ordered in panels versus normalized probe frequency ω_p for the resonance condition $\omega_s = \omega_c$, respectively. The black curves are the transmission functions without cavity protection (compare to fig. (2b)), the red curves are the cavity protected transmission functions, respectively.

Because we effectively removed spins in the vicinity of $\omega_{cp}^{(\pm)}$ which could couple to a radiation field at the frequencies $\omega_{cp}^{(\pm)} \pm 1/2 \cdot \Delta_{cp}$, the absorption of the probe field by the spin distribution is suppressed and the transmission is higher. Most spins are erased by $\varrho_{\text{eff}}^{(\text{rec})}(\omega)$, followed by $\varrho_{\text{eff}}^{(\text{fd})}(\omega)$ and $\varrho_{\text{eff}}^{(\text{q})}(\omega)$ and indeed for all three values of $\Delta_{cp}^{(1,2,3)}$ the transmission of the rectangular distribution is higher than for $\varrho_{\text{eff}}^{(\text{fd,q})}(\omega)$ followed by $\varrho_{\text{eff}}^{(\text{fd})}(\omega)$. All three transmissions are higher than the transmission without cavity protection, depicted in figure (2b), respectively. Note that the full width at half maximum Γ of the two peaks indeed becomes smaller.

As we expected, the loss of spins leads to a reduced effective coupling strength Ω_{eff} with an effective coupling strength $g_{k,\text{eff}}$ for the individual spin and Ω defined in eq. (9c). The FWHM of the two peaks of the absolute value squared of the transmission function in the stationary state (AVSTSS) is a measure for the overlap of the eigenstates of the coupled system and
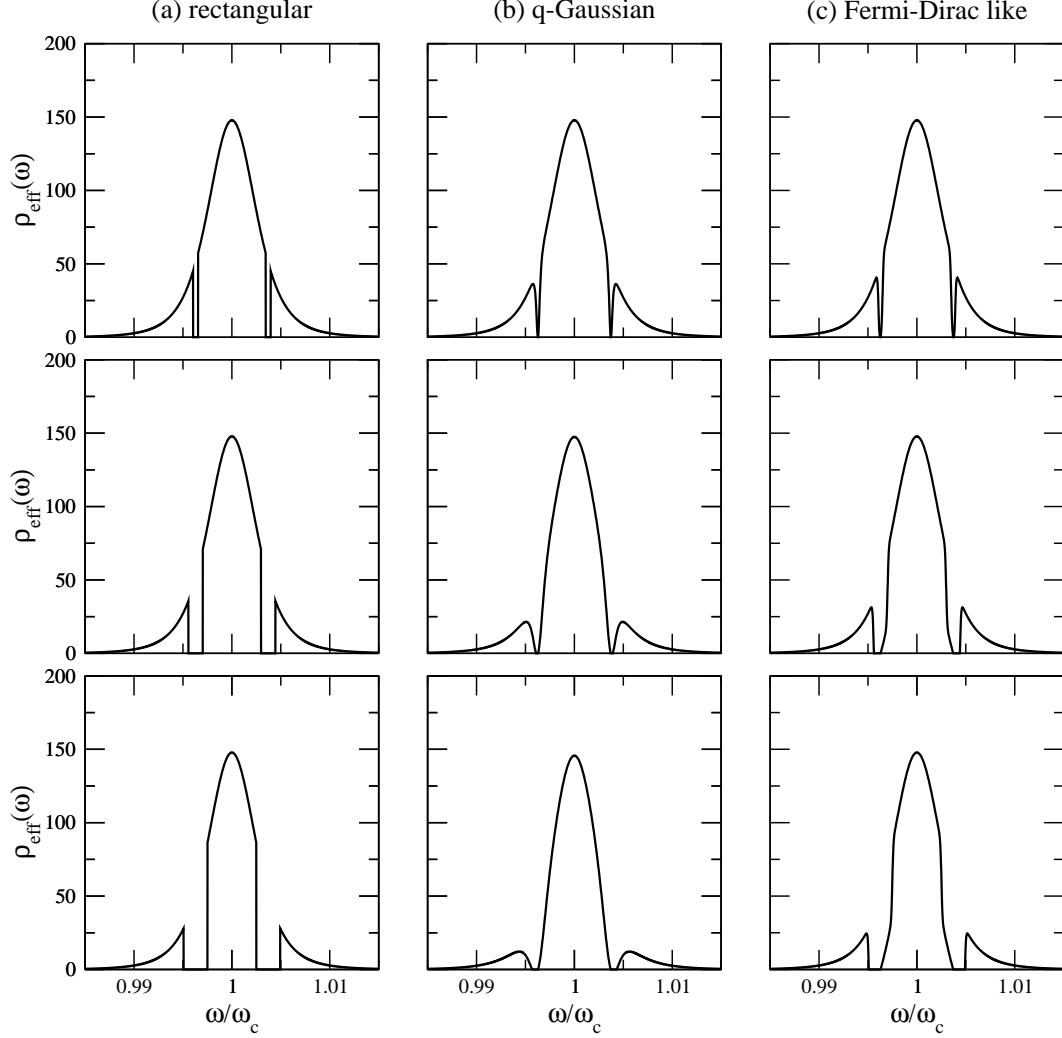
Figure (4)   The effective spin distribution $\varrho_{\text{eff}}^{(\text{rec,q,fd})}(\omega)$ versus normalized frequency ω with $\omega_c = \omega_s$, $\Omega = 2\pi \cdot 10\text{MHz}$ and $\delta\Omega = 0$ for different shapes of $\varrho_{cp}^{(\text{rec,q,fd})}(\omega)$ ordered in columns (a) rectangular distributions eq. (45), (b) q-Gaussian distributions eq. (47) and (c) Fermi-Dirac like distributions eq. (48). $\varrho_{\text{eff}}^{(\text{rec,q,fd})}(\omega)$ for different characteristic widths $\Delta_{cp}^{(1,2,3)}$ is arranged in panels: panel (1) $\Delta_{cp}^{(\text{rec1})} = 2\pi \cdot 1.30\text{MHz}$, $\Delta_{cp}^{(\text{q1})} = 2\pi \cdot 1.06\text{MHz}$, $\Delta_{cp}^{(\text{fd1})} = 2\pi \cdot 1.14\text{MHz}$, panel (2) $\Delta_{cp}^{(\text{rec2})} = 2\pi \cdot 3.90\text{MHz}$, $\Delta_{cp}^{(\text{q2})} = 2\pi \cdot 3.17\text{MHz}$, $\Delta_{cp}^{(\text{fd2})} = 2\pi \cdot 3.90\text{MHz}$ and panel (3) $\Delta_{cp}^{(\text{rec3})} = 2\pi \cdot 6.50\text{MHz}$, $\Delta_{cp}^{(\text{q3})} = 2\pi \cdot 5.28\text{MHz}$, $\Delta_{cp}^{(\text{fd3})} = 2\pi \cdot 6.50\text{MHz}$, respectively. Parameters are listed in tbl. (1).
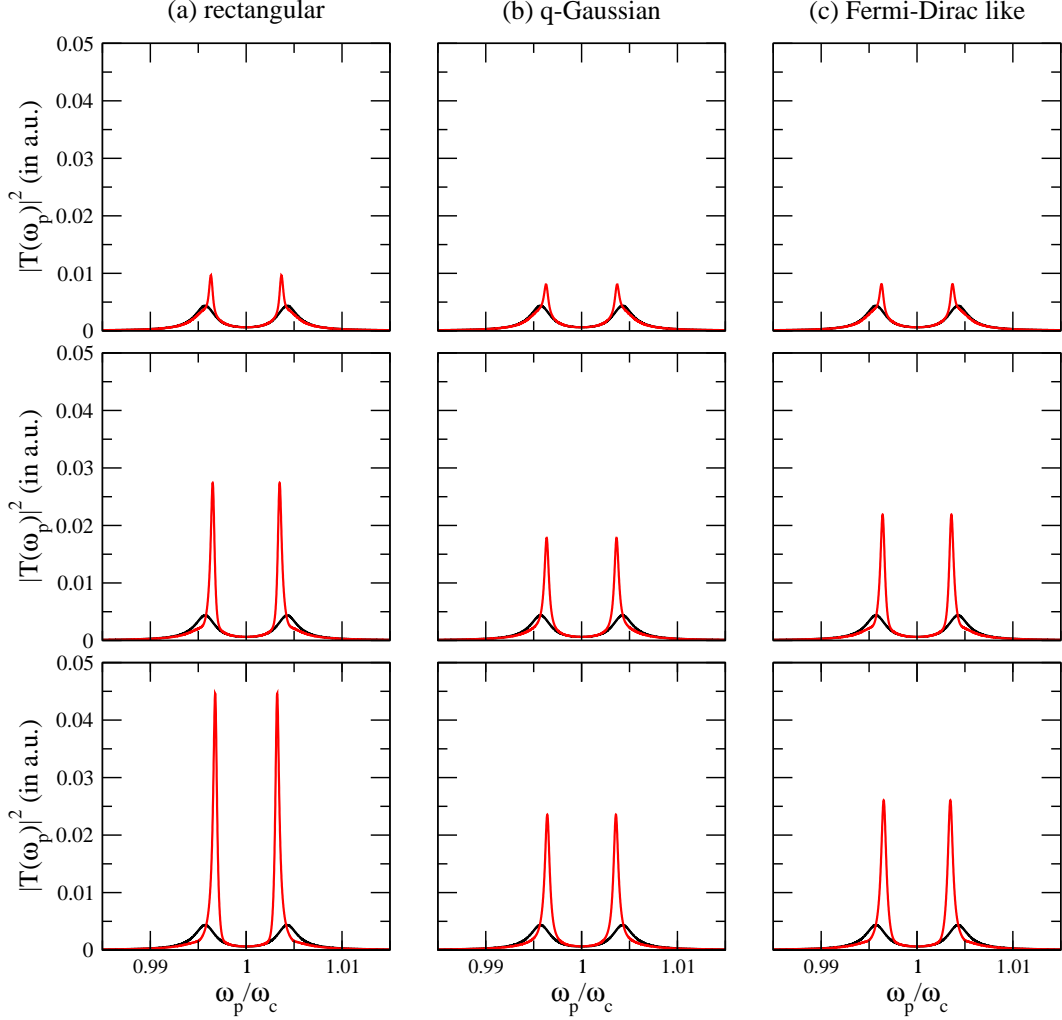
Figure (5) Absolute value squared of the transmission function $|T(\omega_p)|^2$ in the steady-state regime defined by eq. (12) versus normalized probe frequency ω_p with $\omega_s = \omega_c$, $\Omega = 2\pi \cdot 10$MHz and $\delta\Omega = 0$ for different shapes of $\varrho_{cp}^{(\mathrm{rec,q,fd})}(\omega)$ ordered in columns (a) rectangular distributions eq. (45), (b) q-Gaussian distributions eq. (47) and (c) Fermi-Dirac like distributions eq. (48). $|T(\omega_p)|^2$ for different characteristic widths $\Delta_{cp}^{(1,2,3)}$ is arranged in panels: panel (1) $\Delta_{cp}^{(\mathrm{rec1})} = 2\pi \cdot 1.30$MHz, $\Delta_{cp}^{(\mathrm{q1})} = 2\pi \cdot 1.06$MHz, $\Delta_{cp}^{(\mathrm{fd1})} = 2\pi \cdot 1.14$MHz , panel (2) $\Delta_{cp}^{(\mathrm{rec2})} = 2\pi \cdot 3.90$MHz, $\Delta_{cp}^{(\mathrm{q2})} = 2\pi \cdot 3.17$MHz, $\Delta_{cp}^{(\mathrm{fd2})} = 2\pi \cdot 3.90$MHz and panel (3) $\Delta_{cp}^{(\mathrm{rec3})} = 2\pi \cdot 6.50$MHz, $\Delta_{cp}^{(\mathrm{q3})} = 2\pi \cdot 5.28$MHz, $\Delta_{cp}^{(\mathrm{fd3})} = 2\pi \cdot 6.50$MHz, respectively. The black curves are the initial transmission functions without cavity protection, the red curves are the cavity protected transmission functions. Parameters are listed in tbl. (1).

the maxima of the AVSTSS represent the frequencies of the Rabi states, respectively [9, 14]. Since the gap between the maxima of the two peaks (which now is a measure for Ω_{eff}) of the AVSTSS shown in figure (5) becomes smaller, we end up with a modified "effective" ground and excited state of the TLS.

4.3. Time evolution of an excitation in the cavity mode

Now we want to describe the time evolution of the cavity mode $A(t)$ defined by eq. (15) when we apply the cavity protection mechanism described above. We obtain interesting effects by calculating the number of excitations in the cavity mode $A^{\dagger}(t) \cdot A(t)$ defined as $|\langle a(t) \rangle|^2$ with the method of D. Krimer [10] but with a modified spin-distribution $\varrho_{\mathrm{eff}}(\omega)$ given by eq. (38).

Fig. (6) shows $|\langle a(t) \rangle|^2$ versus time for three differently shaped effective spin distributions (rec, q, fd) with three different widths $\Delta_{cp}^{(1,2,3)}/2\pi = (1.3, 3.9, 6.5)\mathrm{MHz}$ for $\Omega = 2\pi \cdot 10\mathrm{MHz}$ and $\delta\Omega = 0$. The black curves are reference curves without cavity protection, the red ones show the behavior of $|\langle a(t) \rangle|^2$ due to the modified spin distributions, respectively.

Although there is a reduction of the effective coupling strength $\Omega_{\mathrm{eff}} < \Omega$ due to the loss of coupling spin components around the frequencies $\omega_{cp}^{(\pm)}$, we can see, that the amplitudes of the Rabi oscillations increase compared to the reference plot (black curves). The dephasing of the Rabi oscillations is suppressed especially for the rectangular distributions where we have less sensitivity for the position of the dips of $\varrho_{\mathrm{eff}}(\omega)$ around $\omega_{cp}^{(\pm)}$, respectively. Due to the smaller Ω_{eff} and the fact, that the period of Rabi oscillations is proportional to $1/\Omega_{\mathrm{eff}}$ [11], [14] we can identify the enhanced period of the red curves in figure (6) with respect to Δ_{cp} as a consequence of the cavity protection mechanism (but this is a trivial consequence).

By using broader widths Δ_{cp} the effects are more pronounced. For $\Delta_{cp}^{(3)} = 6.50$ MHz and the rectangular effective distribution $\varrho_{\mathrm{eff}}^{(\mathrm{rec})}(\omega)$ the first peak of the Rabi oscillation reaches $\approx 85\%$ of the initial value for the number of excitations in the cavity mode $|\langle a(t) \rangle|^2$ compared to $\approx 45\%$ without cavity protection. For $\varrho_{\mathrm{eff}}^{(\mathrm{q,fd})}(\omega)$ we reach $\approx 80\%$ for the number of excitations in the cavity mode $|\langle a(t) \rangle|^2$, compared to the initial value. For the second and third peak of the Rabi oscillation, being barely observable without cavity protection, we see, that for the rectangular case the third peak is still at about 40% of its initial value. This is not far off from $\approx 45\%$ of to the first peak without cavity protection. The damping of the cavity mode is the lowest for the rectangular case, followed by the Fermi-Dirac like and q-Gaussian distribution decreasing with increasing width $\Delta_{cp}^{(1,2,3)}$ of the dips. The biggest damping is observable for the reference plot without cavity protection.

4.4. Variable collective coupling strength

In this section we test the behavior of the time evolution of the cavity mode with respect to different coupling strengths $\Omega/2\pi = (13, 17.5, 22)\mathrm{MHz}$ for the width $\Delta_{cp}/2\pi = 3.9\mathrm{MHz}$ of the cavity protection distributions.

Figure (7) shows the rectangular effective spin distribution defined in the appendix by eq. (45) versus normalized frequency ω for three different collective coupling strengths Ω ordered in columns in panel 1. The absolute value squared of the transmission function given by eq. (12) versus normalized probe-frequency ω_p is depicted in panel 2. The number of excitations in the cavity mode $|\langle a(t) \rangle|^2$ given by eq. (16) versus time for different Ω and the resonance condition $\omega_s = \omega_c = \omega_p$ (without) with rectangular cavity protection and dips located at $\omega_s \pm \Omega$ is shown in (panel 3) panel 4.

In panel 1 the red, blue and green curves denote the effective spin distribution for $\Omega/2\pi = 13, 17.5, 22\mathrm{MHz}$, respectively. In panel 2 the (red, blue, green) and black curves denote the absolute value squared of the transmission function (with) and without cavity protection for $\Omega/2\pi = 13, 17.5, 22\mathrm{MHz}$, respectively. In (panel 3) panel 4 the red, blue and green curves
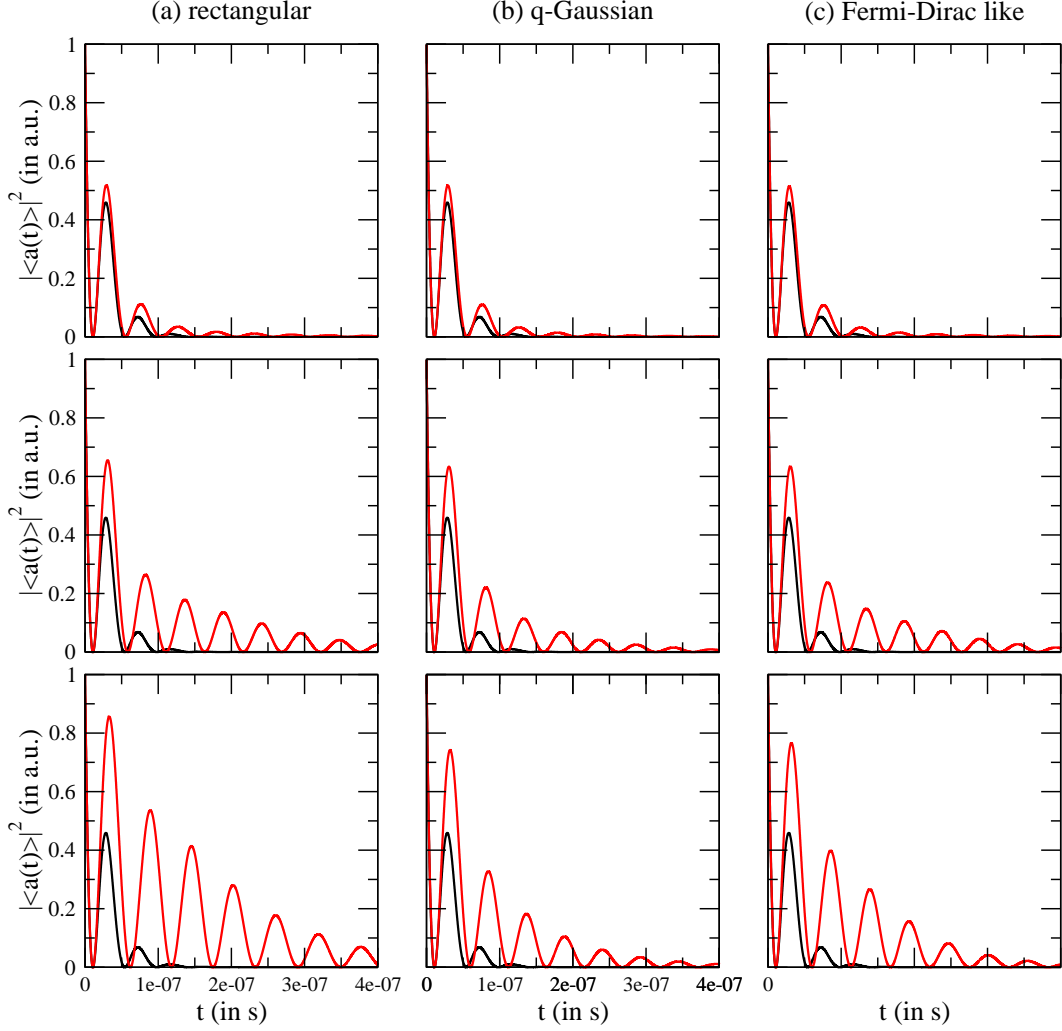
Figure (6) Number of excitations in the cavity mode $|\langle a(t)\rangle|^2$ versus time for the resonance condition $\omega_s = \omega_c = \omega_p$, $\Omega = 2\pi \cdot 10\text{MHz}$ and $\delta\Omega = 0$ for different shapes of $\varrho_{\text{eff}}(\omega)$ ordered in columns (a) rectangular distributions eq. (45), (b) q-Gaussian distributions eq. (47) and (c) Fermi-Dirac like distributions eq. (48) and for different characteristic widths $\Delta_{cp}^{(1,2,3)}$ arranged in panels: panel (1) $\Delta_{cp}^{(\text{rec1})} = 2\pi \cdot 1.30\text{MHz}$, $\Delta_{cp}^{(\text{q1})} = 2\pi \cdot 1.06\text{MHz}$, $\Delta_{cp}^{(\text{fd1})} = 2\pi \cdot 1.14\text{MHz}$, panel (2) $\Delta_{cp}^{(\text{rec2})} = 2\pi \cdot 3.90\text{MHz}$, $\Delta_{cp}^{(\text{q2})} = 2\pi \cdot 3.17\text{MHz}$, $\Delta_{cp}^{(\text{fd2})} = 2\pi \cdot 3.90\text{MHz}$ and panel (3) $\Delta_{cp}^{(\text{rec3})} = 2\pi \cdot 6.50\text{MHz}$, $\Delta_{cp}^{(\text{q3})} = 2\pi \cdot 5.28\text{MHz}$, $\Delta_{cp}^{(\text{fd3})} = 2\pi \cdot 6.50\text{MHz}$ and parameters listed in tbl. (1), respectively. Black curves: $|\langle a(t)\rangle|^2$ without cavity protection, red curves: $|\langle a(t)\rangle|^2$ with cavity protection.

denote the time evolution of $|\langle a(t) \rangle|^2$ for $\Omega/2\pi = 13, 17.5, 22\text{MHz}$ (without) with cavity protection, respectively. The (red, blue, green) and cyan dashed lines in panel 3 and 4 describe the decay of the Rabi-Oscillations for $\Omega/2\pi = (13, 17.5, 22)\text{MHz}$ and the limiting decay given by eq. (36), respectively.

We can see, that for all three values of Ω we almost reach the limiting decay rate by using a characteristic width $\Delta_{cp}/2\pi = 3.9\text{MHz}$. For the lower two values of Ω the initial decay is faster than for $\Omega/2\pi = 22\text{MHz}$, but the asymptotic decay is similar. By increasing the coupling strength Ω, we clearly see, that we erase fewer spins from the spectral distribution than for smaller Ω (as we do so in the vicinity of $\omega_s \pm \Omega$) and we find, that we more and more approach the limiting decay rate given by eq. (35). We obtain a remarkably increased lifetime of the Rabi-oscillations compared to the reference behavior without protection although we alter $\varrho(\omega)$ only in a very narrow interval. After an initial decay, which is comparable to the unprotected case, we find an asymptotic decay which is comparable to the limiting decay given by eq. (36). When we compare the effect of increasing Ω with the initial distribution (which corresponds to the cavity protection mechanism of Diniz et al. in [9]) to an increasing Ω and a modified effective spin distribution, we find for the latter, that we almost reach the limiting decay for finite Ω while it remains a limit for Diniz et al. when we use a q-Gaussian spin distribution. So we expect the mechanism of modifying the inhomogeneous spin distribution to be more effective for cavity protection as only increasing the collective coupling strength Ω.

Figure (8) shows the behavior of the system with $\Omega/2\pi = 22\text{MHz}$ and $\delta\Omega = 0$ for three different effective distributions ordered in columns (a) rectangular (red), (b) q-Gaussian (blue) and (c) Fermi-Dirac like (green) in panel 1. In panel 2 the absolute value squared of the transmission function is plotted for $\varrho_{\text{eff}}^{(\text{rec,q,fd})}(\omega)$ in the colors (red, blue, green) and the black curves are the transmission functions without cavity-protection. Panel 3 shows the time evolution of $|\langle a(t) \rangle|^2$ for no protection (black) and with rectangular (red), q-Gaussian (blue) and the Fermi-Dirac like (green) cavity protection for the resonance condition $\omega_s = \omega_c = \omega_p$ and parameters listed in tbl. (1). The dashed lines denote the effective decay of the Rabi oscillations, respectively.

Again we see remarkable effects due to the erased spins in the spectral density of the emitters. Even for the q-Gaussian distribution, where we erased the fewest amount of emitters, we find a significantly reduced decay rate of the excitation in the cavity mode.

Figure (9) shows the behavior with $\Omega/2\pi = 22\text{MHz}$ and $\delta\Omega = 0$ for three different characteristic widths $\Delta_{cp}^{(1)}/2\pi = 1.3\text{MHz}$ (red), $\Delta_{cp}^{(2)}/2\pi = 3.9\text{MHz}$ (blue) and $\Delta_{cp}^{(3)}/2\pi = 6.5\text{MHz}$ (green) and rectangular cavity protection. Panel 1 shows $\varrho_{\text{eff}}^{(\text{rec})}(\omega)$ for all three widths ordered in columns $\Delta_{cp}^{(1)}$ (a), $\Delta_{cp}^{(2)}$ (b) and $\Delta_{cp}^{(3)}$ (c), respectively. In panel 2 the absolute value squared of the transmission function is plotted for $\varrho_{\text{eff}}^{(\text{rec})}(\omega)$ ordered in columns for different widths $\Delta_{cp}^{(1)}$ (red), $\Delta_{cp}^{(2)}$ (blue) and $\Delta_{cp}^{(3)}$ (green) and the black curve shows $|T(\omega_p)|^2$ without cavity-protection. Panel 3 shows the time evolution of $|\langle a(t) \rangle|^2$ without protection (black) and with cavity protection for $\Delta_{cp}/2\pi = (1.3, 3.9, 6.5)\text{MHz}$ (red, blue, green) for the resonance condition $\omega_s = \omega_c = \omega_p$ and parameters listed in tbl. (1). The dashed lines denote the effective decay of the Rabi oscillations, respectively.

We see that we get the best results, when we use broader dips although the asymptotic decay is similar for the bigger two values of Δ_{cp}. The dips should not be too broad, because we don't want to remove the whole spin distribution but remain in the strong coupling regime. We assume, that one should ensure, that the dips of the effective spin distribution at least contain the characteristic width of the absolute value squared of the transmission function with respect to the spectral range in frequency.
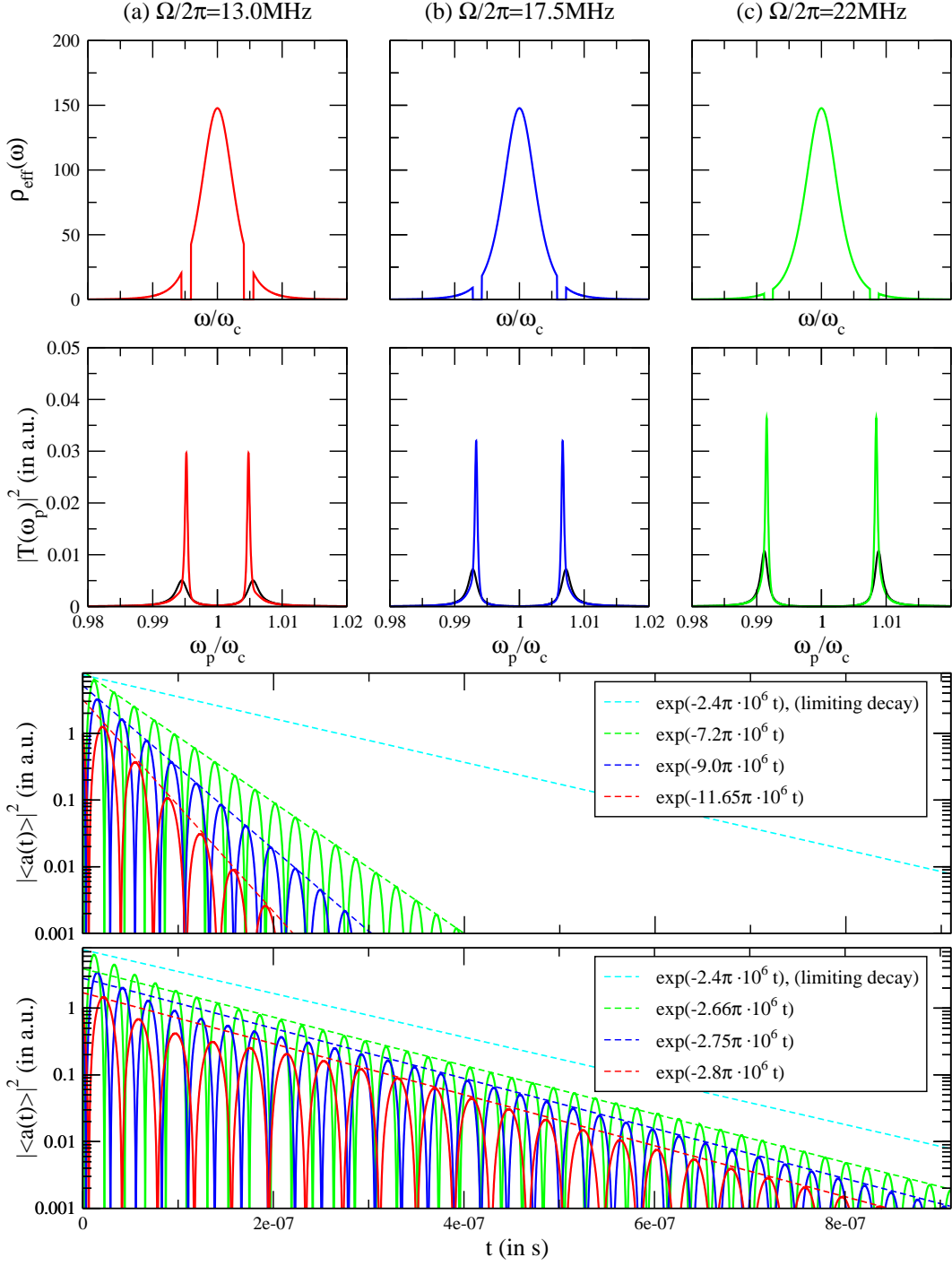
Figure (7) Behavior for different collective coupling strengths Ω for rectangular cavity protection. The dips are located at $\omega_s \pm \Omega$, $\delta\Omega = 0$, $\Delta_{cp} = 2\pi \cdot 3.9\text{MHz}$ and parameters in tbl. (1). The first panel shows the effective spectral spin distribution with dips in the vicinity of $\omega_s \pm \Omega$ for different Ω (colored), respectively. The second panel shows the absolute value squared of the transmission function according to the effective spin distributions (colored) compared to the transmission function without cavity protection (black). The third panel shows the time evolution of the excitation in the cavity mode $|\langle a(t) \rangle|^2$ without and the fourth panel with cavity protection for the resonance condition $\omega_s = \omega_c = \omega_p$ and different collective coupling strengths Ω (colored) with according effective decay (dashed colored) compared to the limiting decay (cyan dashed) defined by eq. (36).
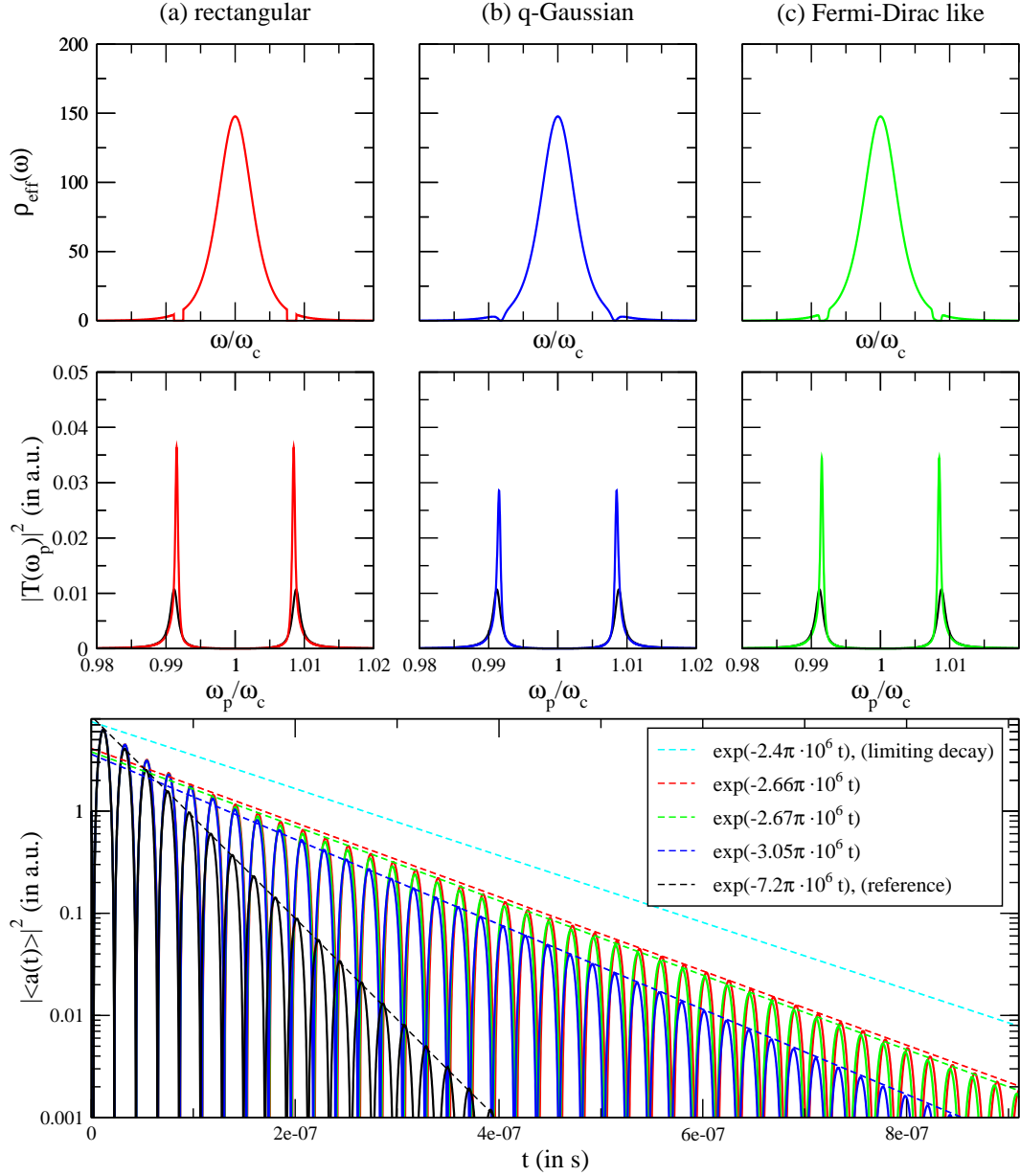
Figure (8)   Behavior for different cavity-protection distributions $\varrho_{\mathrm{eff}}^{(\mathrm{rec,q,fd})}(\omega)$ with $\Omega = 2\pi \cdot 22\mathrm{MHz}$, dips at $\omega_s \pm \Omega$, $\delta\Omega = 0$, $\Delta_{cp} = 2\pi \cdot 3.9\mathrm{MHz}$ and parameters in tbl. (1). The first panel shows the effective spectral spin distribution with dips in the vicinity of $\omega_s \pm \Omega$ for different shapes of the cavity protection distribution (colored), respectively. The second panel shows the transmission function according to the effective spin distributions (colored) compared to the transmission function without cavity protection (black). The third panel shows the time evolution of the excitation in the cavity mode with cavity protection for the resonance condition $\omega_s = \omega_c = \omega_p$ and different shapes of the cavity protection distribution (colored) with effective decay (dashed colored) compared to $|\langle a(t)\rangle|^2$ without cavity protection (black) and to the limiting decay (cyan dashed) defined in eq. (36).
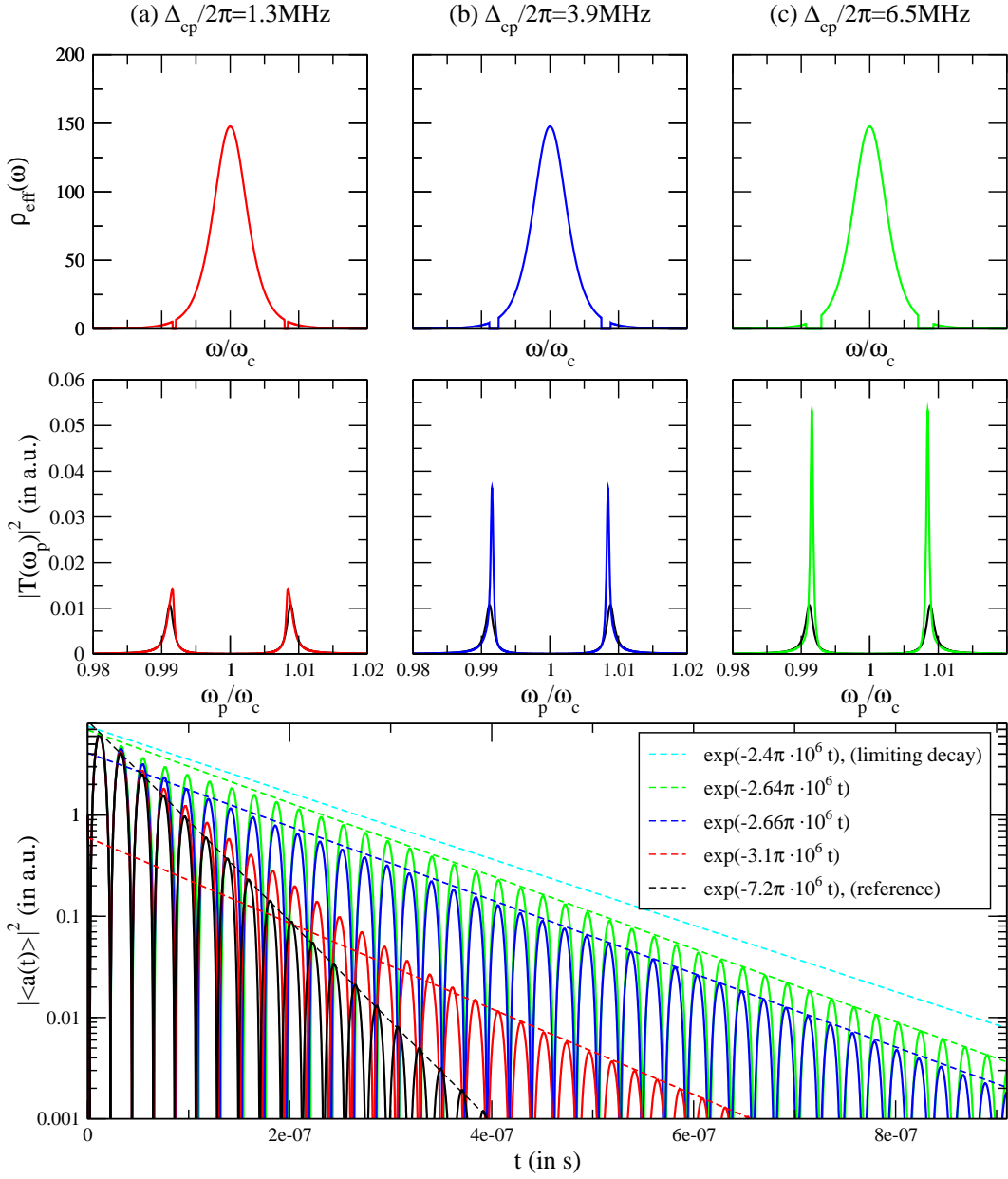
Figure (9) Behavior for rectangular spin distribution with variable characteristic width Δ_{cp}, $\delta\Omega = 0$, $\Omega = 2\pi \cdot 22\text{MHz}$, dips located at $\omega_s \pm \Omega$ and parameters in tbl. (1). The first panel shows the effective spectral spin distribution with dips in the vicinity of $\omega_s \pm \Omega$ for different width of the holes Δ_{cp} (colored), respectively. The second panel shows the absolute value squared of the transmission function according to the effective spin distributions (colored) compared to the transmission function without cavity protection (black). The third panel shows the time evolution of the excitation in the cavity mode $|\langle a(t)\rangle|^2$ with cavity protection for the resonance condition $\omega_s = \omega_c = \omega_p$ and different widths of the dips Δ_{cp} (colored) with effective decay (dashed colored) compared to $|\langle a(t)\rangle|^2$ without cavity protection (black) and to the limiting decay (cyan dashed) defined in eq. (36).

4.5. Cavity protection dips at effective coupling strength

The effective loss of spins due to the modified inhomogeneous spin distribution leads to an decreased effective coupling strength $\Omega_{\text{eff}} < \Omega$. The gap between the peaks of the transmission function thus will get smaller which, in turn, will lead to an alternated avoided crossing. This also leads to slightly modified ground-level and excited dressed states of the coupled solid matter TLS and the cavity-mode in the strong coupling regime. In the previous sections we saw, that an effect due to the cavity protection mechanism is clearly observable. Now we want to check if we get an even better effect, when we locate the dips of the effective spin distribution at precisely the frequencies of the effective coupling strength $\omega_{\text{eff}}^{(\pm)} = \omega_s \pm \Omega_{\text{eff}}$ and not at the original coupling strength $\omega_{cp}^{(\pm)} = \omega_s \pm \Omega$. Ω_{eff} is considered as $1/2$ the gap between the two maxima of the absolute value squared of the transmission function. Note that this is an iterative problem, because a modified effective spin distribution, with respect to a small variation of the position of the dips by $\delta\Omega$, will also change the position of the two maxima of the transmission function.

Figure (10) shows the behavior of the system with $\Omega/2\pi = 22$MHz for three different characteristic widths $\Delta_{cp}^{(1,2,3)}/2\pi = (1.3, 3.9, 6.5)$MHz ordered in columns ((a) red, (b) blue,(c) green) and the dips of the rectangular effective spin distribution located at precisely $\omega_{\text{eff}}^{(\pm)}$, respectively. Panel 1 shows $\varrho_{\text{eff}}^{(\text{rec})}(\omega)$ with dips at $\omega_{\text{eff}}^{(\pm)}$ for all three widths, respectively. In panel 2 the absolute value squared of the transmission function is depicted for the dips located at $\omega_{\text{eff}}^{(\pm)}$ and $\Delta_{cp}/2\pi = 1.3$MHz (red), $\Delta_{cp}/2\pi = 3.9$MHz (blue) and $\Delta_{cp}/2\pi = 6.5$MHz (green) and the black curves show $|T(\omega_p)|^2$ without cavity-protection. Note that the range of the horizontal-axis for panel 1 and 2 is plotted from $\omega_{(p)}/\omega_c = 0.988$ to $\omega_{(p)}/\omega_c = 0.995$ and shows only a part of the left branch of the functions but in a higher resolution. Panel 3 shows $|\langle a(t)\rangle|^2$ versus time for the resonance condition $\omega_s = \omega_p = \omega_c$ and $\Delta_{cp}^{(1)}/2\pi = 1.3$MHz with the dips located at $\omega_{cp}^{(\pm)}$ (red curve) and at the effective coupling strength $\omega_{\text{eff}}^{(\pm)}$ (red dashed curve). The black (dashed) line denotes the decay of $|\langle a(t)\rangle|^2$ for the dips located at $\omega_{cp}^{(\pm)}$ ($\omega_{\text{eff}}^{(\pm)}$), the blue line denotes the initial decay for both cases. Panel 4 shows $|\langle a(t)\rangle|^2$ versus time for the resonance condition $\omega_s = \omega_p = \omega_c$ for $\Delta_{cp}^{(2,3)}/2\pi = (3.9, 6.5)$MHz (blue,green) and the dips located at $\omega_{cp}^{(\pm)}$ (filled curves) and at the effective coupling strength $\omega_{\text{eff}}^{(\pm)}$ (dashed curves). The decay rates of $|\langle a(t)\rangle|^2$ for $\Delta_{cp}^{(2,3)}/2\pi = (3.9, 6.5)$MHz and the dips located at $\omega_{cp}^{(\pm)}$ and $\omega_{\text{eff}}^{(\pm)}$ are very similar and can be taken from figure (9). The cyan dashed line is the limiting decay from eq. (36).

We can see that only for small widths Δ_{cp} there is an observable effect due to the dips of $\varrho_{\text{eff}}(\omega)$ being located at $\omega_s \pm \Omega_{\text{eff}}$ compared to $\omega_s \pm \Omega$. When one uses broader widths it doesn't make a difference, if the holes are located at $\omega_{\text{eff}}^{(\pm)}$ or $\omega_{cp}^{(\pm)}$ as long as the maxima of the transmission function are located within the intervals where $\varrho_{\text{eff}}(\omega) = 0$. This can be seen in panel 4 of figure (10). Note that in figure (6) $\Delta_{cp}^{(3)} = 2\pi \cdot 6.5$MHz and $\Omega = 2\pi \cdot 10$MHz are of the same magnitude and by further increasing of Δ_{cp} we more and more erase the complete spin distribution. In this case, the effects may occur because of an effective decreased FWHM $\gamma_{q,\text{eff}}$ of the spin ensemble which as well leads to an enhanced lifetime as long as the system remains in the strong coupling regime. So we did some calculations for variable positions of the dips by using different $\delta\Omega$ with $|\delta\Omega| < \Omega$ for different fixed Ω. Even though one may find the first 2-3 peaks of the Rabi oscillations to be bigger for the dips located at $\omega_s \pm (\Omega - |\delta\Omega|)$, $\omega_{\text{eff}}^{(\pm)} = \omega_s \pm \Omega_{\text{eff}}$ seems to be the best choice to improve the asymptotic decay rate. The cavity protection mechanism described in this thesis may be interpreted in a way, that removing a narrow spectral interval of spins around the frequencies $\omega_s \pm \Omega$ (for better observable effects by smaller dip-widths at $\omega_s \pm \Omega_{\text{eff}}$) leads to a suppressed coupling of the ground and excited Rabi state with the inhomogeneous spin-environment at the frequencies $\omega_s \pm \Omega$ and with the continuum of eigenstates of the Hamiltonian due to a reduced overlap of the Rabi states with the other eigenstates.
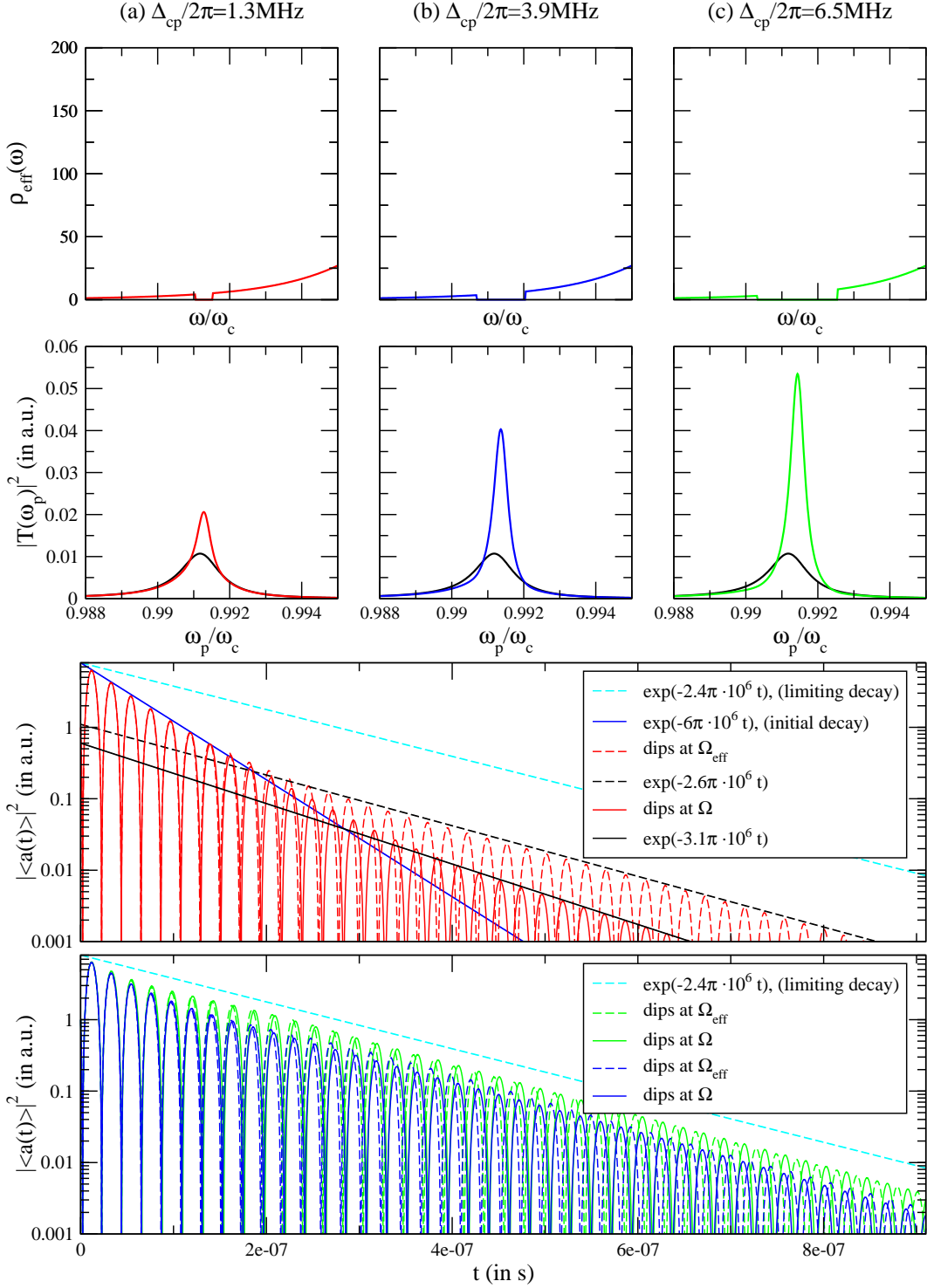
Figure (10) Behavior for rectangular spin distribution and for different widths $\Delta_{cp}^{(1,2,3)}$ of the dips, $\Omega = 2\pi \cdot 22$MHz, dips located at $\omega_s \pm \Omega_{\text{eff}}$ and parameters in tbl. (1). The first panel shows the effective spectral spin distribution with dips at $\omega_s \pm \Omega_{\text{eff}}$ (colored) and the second the absolute value squared of the transmission function in the vicinity of $\omega_s - \Omega$ for different dip-widths $\Delta_{cp}^{(1,2,3)}$ (colored) and without cavity protection (black), respectively. The third panel corresponds to $\Delta_{cp}^{(1)}/2\pi = 1.3$MHz, the fourth to $\Delta_{cp}^{(2,3)}/2\pi = (3.9, 6.5)$MHz. They show the time evolution of the excitation in the cavity mode $|\langle a(t) \rangle|^2$ with cavity protection and dips located at $\omega_s \pm \Omega_{\text{eff}}$ (colored dashed) and $\omega_s \pm \Omega$ (colored) for the resonance condition $\omega_s = \omega_c = \omega_p$ and different widths Δ_{cp} compared to the limiting decay defined by eq. (36).

5. Conclusions and Outlook

In conclusion, we treated an inhomogeneously broadened ensemble of N two level systems as a continuous bosonic spin distribution modeling it by a q-Gaussian distribution centered at a mean frequency ω_s with a full width at half maximum (FWHM) γ_q. This spin ensemble couples with a collective coupling strength Ω to a cavity mode and the whole system behaves like two coupled, but damped harmonic oscillators where the energy is exchanged in a coherent way. The inhomogeneous broadening of the emitters causes an overlap of the Rabi-states with a continuum of eigenstates of the Hamiltonian. This leads to a dephasing of the Rabi oscillations between the excited and ground state of the coupled two level system additionally to the cavity and spin losses and thus to an enhanced decay rate when the system is initially excited. The system therefore loses energy due to the cavity losses, individual spin losses and due to the inhomogeneous broadening of the spin distribution.

We now erased a small spectral range from the inhomogeneously broadened spectral density of the emitters in the vicinity of the frequencies $\omega_s \pm \Omega$, respectively, still remaining in the strong coupling regime. Following this procedure, we effectively suppressed the action of the inhomogeneous broadening of the spin distribution on the dephasing of the Rabi oscillations since we reduced the overlap of the Rabi states with the continuum of eigenstates of the Hamiltonian. With our cavity protection mechanism we obtain a remarkably increased lifetime of the Rabi-oscillations as compared to the reference behavior without protection although we alter the spin distribution only in narrow intervals. We almost reach the limiting decay given by the cavity and single spin losses when we increase, but keep a finite collective coupling strength. We also found, that width and shape of the dips in the effective spin distribution have dramatic effects on the behavior of the system. The broader the dips, the better the results, as long as we do not erase too many spins and stay in the strong coupling regime. The FWHM of the two peaks of the absolute value squared of the transmission function in the stationary state (AVSTSS) is a measure for the overlap of the eigenstates of the coupled system and the maxima of the AVSTSS represent the frequencies of the Rabi states, respectively. We therefore suggest, that the mean frequencies of the cavity protection intervals should match with the maxima of the AVSTSS and that the dips should at least cover the FWHM of the two peaks of the AVSTSS. Furthermore, we obtained the best results for cavity protection, when we used rectangular shaped dips where the modified spin distribution becomes zero on an interval around the frequencies corresponding to the Rabi states, respectively. We never observed a decay rate which was smaller than the limiting decay rate.

The cavity protection mechanism described in this thesis is a very good option to enhance the lifetime of Rabi oscillations in the coupled system of cavity mode and spin ensemble when Ω is of the same magnitude as γ_q. We believe, that one can realize such a modified spin distribution by pumping a narrow band of the spectral density of the emitters into permanent excitation by irradiating the NV-Center diamond with a laser of frequency $\omega_{cp}^{(\pm)} \approx \omega_s \pm \Omega$, respectively. When all spins are excited in the vicinity of $\omega_{cp}^{(\pm)}$, we effectively burned two holes into the continuous spin distribution and the laser should be turned off to avoid further thermal excitation. By doing so, we prepare the diamond in a proper way such that the modified inhomogeneous spin ensemble should provide the minimal decay rate in a subsequent experiment.

A. Numerical solution of the Volterra integral equation

The integral equation eq. (16) for $\tilde{A}(t)$ consists of an integral over the product of $\mathcal{K}(t-\tau)$ and $\tilde{A}(\tau)$ from $\tau = 0$ to $\tau = t$ and an additional function $\mathcal{F}(t)$, which appears due to the nontrivial initial conditions. We see that $\tilde{A}(t)$ depends on all former solutions of $\tilde{A}(\tau)$ with $\tau < t$, but also on the value of $\tilde{A}(t)$ at the time $\tau = t$ and thus the cavity mode $A(t)$ given by eq. (15) is a nontrivial quantity. The integration from $\tau = 0$ to $\tau = t$ in eq. (16) is performed numerically by defining $n-1$ proper time steps $\Delta t = t_n/(n-1)$ and replacing the time integration from $\tau = 0 = t_1$ to $\tau = t = t_n$ with a sum of integrals for every step $\tau = t_m$ to $\tau = t_{m+1}$

$$\tilde{A}(t_n) = \sum_{m=1}^{n-1} \int_{t_m}^{t_{m+1}} \mathcal{K}(t_n - \tau)\tilde{A}(\tau)d\tau + \mathcal{F}(t_n). \tag{40}$$

Then we use the trapezoid formula on every single integration

$$
\begin{aligned}
\tilde{A}(t_n) &= \sum_{m=1}^{n-1} \frac{\mathcal{K}(t_n - t_m)\tilde{A}(t_m) + \mathcal{K}(t_n - t_{m+1})\tilde{A}(t_{m+1})}{2} \cdot \Delta t + \mathcal{F}(t_n) \\
&= \frac{\Delta t}{2} \cdot \left\{ \sum_{m=1}^{n-1} \mathcal{K}(t_n - t_m)\tilde{A}(t_m) + \sum_{j=2}^{n} \mathcal{K}(t_n - t_j)\tilde{A}(t_j) \right\} + \mathcal{F}(t_n) \\
&= \frac{\Delta t}{2} \cdot \left\{ 2\sum_{m=2}^{n-1} \mathcal{K}(t_n - t_m)\tilde{A}(t_m) + \mathcal{K}(t_n - t_1)\tilde{A}(t_1) + \mathcal{K}(t_n - t_n)\tilde{A}(t_n) \right\} + \mathcal{F}(t_n) \\
&= \Delta t \cdot \left\{ \sum_{m=2}^{n-1} \mathcal{K}(t_n - t_m)\tilde{A}(t_m) + \frac{1}{2} \cdot \mathcal{K}(t_n - t_1)\tilde{A}(t_1) \right\} + \frac{\Delta t}{2} \cdot \mathcal{K}(t_n - t_n)\tilde{A}(t_n) + \mathcal{F}(t_n).
\end{aligned}
\tag{41}
$$

Now we can rewrite eq. (41) and find an expression for $\tilde{A}(t_n)$ for the time t_n with initial condition $t_1 = 0$

$$\tilde{A}(t_n) = \frac{\Delta t \cdot \left\{ \sum_{m=2}^{n-1} \mathcal{K}(t_n - t_m)\tilde{A}(t_m) + \frac{1}{2} \cdot \mathcal{K}(t_n - t_1)\tilde{A}(t_1) \right\} + \mathcal{F}(t_n)}{1 - \frac{\Delta t}{2}\mathcal{K}(0)}, \tag{42}$$

and with an appropriate small step size Δt and enough steps n for the iteration we can calculate $\tilde{A}(t_n)$ precisely at pleasure.

B. Cavity protection modeling

In this section we describe, how the cavity-protection distributions are modeled and what conditions have to be made.

B.1. Cavity protection conditions

We defined an *effective spin distribution* $\varrho_{\text{eff}}(\omega)$ with two dips at $\omega_{cp}^{(\pm)} = \omega_s \pm (\Omega + \delta\Omega)$ with full (dip-)width Δ_{cp}, respectively, by eq. (38) and eq. (39). $\delta\Omega$ is a small variation of the position of the dips. To form this effective distribution we subtract another distribution from the initial spectral density $\varrho(\omega)$ defined in eq. (10), the *cavity protection distribution* $\varrho_{cp}(\omega)$. We will identify the frequencies $\omega_{cp}^{(-)} = \omega_s - (\Omega + \delta\Omega)$ and $\omega_{cp}^{(+)} = \omega_s + (\Omega + \delta\Omega)$ as mean frequency of the left and right branch of the cavity protection distribution, respectively.

When we talk about both dips, we will simply write $\omega_{cp}^{(\pm)} = \omega_s \pm (\Omega + \delta\Omega)$. To find a proper expression for $\varrho_{\mathrm{cp}}(\omega)$ we define the following conditions

$$\varrho_{cp}(\omega_{cp}^{(\pm)}) = \varrho(\omega_{cp}^{(\pm)}), \tag{43a}$$

$$\varrho_{cp}(\omega) = 0, \text{ for } \omega \notin \omega_{cp}^{(\pm)} \pm \frac{1}{2}\Delta_{cp}. \tag{43b}$$

This means, that $\varrho_{cp}(\omega)$ should only be non-zero in the intervals $\omega_{cp}^{(\pm)} \pm \Delta_{cp}/2$ and should erase all the spins in the vicinity of $\omega_{cp}^{(\pm)}$, respectively. When $\varrho(\omega)$ is symmetric then $\varrho_{cp}(\omega)$ and $\varrho_{\mathrm{eff}}(\omega)$ are symmetric too with respect to ω_s.

To be more insensitive with respect to the position $(\omega_{cp}^{(\pm)})$ and shape (superscript (x) = (rec, q, fd)) of the dips, we introduce three different shapes for the cavity protection distribution $\varrho_{cp}^{(\mathrm{x})}(\omega)$: the *rectangular distribution* denoted as $\varrho_{cp}^{(\mathrm{rec})}(\omega)$, a more narrow *q-Gaussian distribution* $\varrho_{cp}^{(\mathrm{q})}(\omega)$ and a more rectangular *Fermi-Dirac like distribution* $\varrho_{cp}^{(\mathrm{fd})}(\omega)$. Specific shapes of the effective distributions will be defined analogue as $\varrho_{\mathrm{eff}}^{(\mathrm{x})}(\omega)$. If we do not refer to a particular shape we will write $\varrho_{cp}(\omega)$ and $\varrho_{\mathrm{eff}}(\omega)$.

To make sure $\varrho_{cp}(\omega)$ satisfies the condition (43b) we can't use Δ_{cp} as full width for every cavity protection distribution defined above. We have to make some specifications of how precise the conditions have to be fulfilled because $\varrho_{\mathrm{eff}}^{(\mathrm{q})}(\omega)$ and $\varrho_{\mathrm{eff}}^{(\mathrm{fd})}(\omega)$ are analytical expressions which can become very small outside the ranges $\left[\omega_{cp}^{(\pm)} - 1/2\Delta_{cp}, \omega_{cp}^{(\pm)} + 1/2\Delta_{cp}\right]$ but do not completely vanish. For his purpose the height Δ_ϱ and width Δ_ω determine a window, where $\varrho_{\mathrm{eff}}(\omega)$ has to be in a certain shape. Out of that we have to numerically calculate the widths $\Delta_{cp}^{(\mathrm{q})}$ and $\Delta_{cp}^{(\mathrm{fd})}$ for the q-Gaussian and Fermi-Dirac like distribution, respectively. The specifying conditions write as follows

$$\varrho_{cp}^{(\mathrm{x})}\left(\omega_{cp}^{(-)} - \frac{1}{2}(\Delta_{cp} + \Delta_\omega)\right) \leq \Delta_\varrho, \tag{44a}$$

$$\varrho_{cp}^{(\mathrm{x})}\left(\omega_{cp}^{(-)} - \frac{1}{2}(\Delta_{cp} - \Delta_\omega)\right) > \Delta_\varrho, \tag{44b}$$

$$\varrho_{cp}^{(\mathrm{x})}\left(\omega_{cp}^{(+)} + \frac{1}{2}(\Delta_{cp} - \Delta_\omega)\right) > \Delta_\varrho, \tag{44c}$$

$$\varrho_{cp}^{(\mathrm{x})}\left(\omega_{cp}^{(+)} + \frac{1}{2}(\Delta_{cp} + \Delta_\omega)\right) \leq \Delta_\varrho. \tag{44d}$$

Eqs. (44a,44d) determine that $\varrho_{cp}(\omega)$ starts small enough around $\omega_{cp}^{(-)} - \frac{1}{2}(\Delta_{cp} + \Delta_\omega)$ and $\omega_{cp}^{(+)} + \frac{1}{2}(\Delta_{cp} + \Delta_\omega)$, respectively. Eqs. (44b,44c) make sure, that $\varrho_{cp}(\omega)$ will rise around $\omega_{cp}^{(-)} - \frac{1}{2}(\Delta_{cp} - \Delta_\omega)$ and $\omega_{cp}^{(+)} + \frac{1}{2}(\Delta_{cp} - \Delta_\omega)$ with our specified horizontal (Δ_ω) and vertical precision (Δ_ϱ) and thus serve a significant value for the effective spin distribution, respectively.

In this report the width Δ_ω is taken to be small and the height Δ_ϱ of the window is fixed to $1/e \cdot \varrho(\omega_{cp}^{(\pm)})$. This ensures, that Δ_{cp} can be treated as characteristic width of the cavity protection distribution (or of the dips of the effective distribution), respectively. Now we can compare the effects of the modified effective spin distributions with respect to the characteristic widths of the cavity protection distributions and thus to the amount of erased spins, respectively.

B.2. The rectangular cavity protection distribution

The rectangular cavity protection distribution simply describes the removal of all the spins in the intervals $\omega \in \left[\omega_{cp}^{(\pm)} - \frac{1}{2}\Delta_{cp}^{(\mathrm{rec})}, \ \omega_{cp}^{(\pm)} + \frac{1}{2}\Delta_{cp}^{(\mathrm{rec})}\right]$, respectively. The rest of $\varrho(\omega)$ remains

untouched. Therefore $\varrho_{cp}^{(\text{rec})}(\omega)$ should show if cavity protection is possible in principal by removing a narrow spectral band of the continuous spectral spin distribution around the frequencies corresponding to the Rabi states, respectively.

$$\varrho_{cp}^{(\text{rec})}(\omega) = \begin{cases} \varrho(\omega), \text{ for } \omega \in \left[\omega_{cp}^{(\pm)} - \frac{1}{2}\Delta_{cp}^{(\text{rec})}, \omega_{cp}^{(\pm)} + \frac{1}{2}\Delta_{cp}^{(\text{rec})}\right] \\ \\ 0, \text{ otherwise} \end{cases} \tag{45}$$

We can also write Δ_{cp} for $\Delta_{cp}^{(\text{rec})}$.

B.3. The q-Gaussian cavity-protection distribution

For $\varrho(\omega)$ and $\omega_{cp}^{(\pm)}$ being symmetrical around ω_s, we simply add two q-Gaussian distributions which are, respectively, centered around $\omega_{cp}^{(\pm)}$

$$\tilde{\varrho}_{cp}^{(q)}(\omega) = A \cdot \left(\left[1 - (1 - q_{cp})\frac{(\omega - \omega_{cp}^{(-)})^2}{(\Delta_{cp}^{(q)})^2} \right]^{\frac{1}{1 - q_{cp}}} \right.$$
$$\left. + \left[1 - (1 - q_{cp})\frac{(\omega - \omega_{cp}^{(+)})^2}{(\Delta_{cp}^{(q)})^2} \right]^{\frac{1}{1 - q_{cp}}} \right) \tag{46}$$

where $\gamma_{cp}^{(q)} = 2\Delta_{cp}^{(q)}\sqrt{\dfrac{2^{q_{cp}} - 2}{2q_{cp} - 2}}$ is the full width at half maximum (FWHM). q_{cp} is listed in tbl. (1). These two Distributions will drop against zero and won't affect each other in a significant way, when one chooses the right parameters. We however have to consider, that we can't use the characteristic width of the cavity protection Δ_{cp} as width $\Delta_{cp}^{(q)}$ in eq. (46) to fulfill the conditions (44). $\Delta_{cp}^{(q)}$ is numerically calculated out of the boundary-conditions (44) to determine, that $\varrho_{cp}^{(q)}(\omega)$ only (significantly) effects $\varrho(\omega)$ in the specified intervals $\left[\omega_{cp}^{(\pm)} - \frac{1}{2}\Delta_{cp}, \omega_{cp}^{(\pm)} + \frac{1}{2}\Delta_{cp}\right]$, respectively. The intervals may overlap as well, if one wants to observe that case. The normalization factor A vanished, when we scale $\tilde{\varrho}_{cp}^{(q)}(\omega)$ to

$$\varrho_{cp}^{(q)}(\omega) = \tilde{\varrho}_{cp}^{(q)}(\omega) \cdot \frac{1}{2}\left(\frac{\varrho(\omega_{cp}^{(-)})}{\tilde{\varrho}_{cp}^{(q)}(\omega_{cp}^{(-)})} + \frac{\varrho(\omega_{cp}^{(+)})}{\tilde{\varrho}_{cp}^{(q)}(\omega_{cp}^{(+)})} \right), \tag{47}$$

to fulfill the cavity protection condition (43a). Although the problem is symmetrical around ω_s we took the average value for the normalization because the calculation of the cavity-protection density has been done numerically so there could be a slightly different height and position of the peaks of the two added distributions.

B.4. The Fermi-Dirac like cavity protection distribution

To describe a smooth distribution but be more insensitive for the positions $\omega_{cp}^{(\pm)}$ of the dips in the effective distribution $\varrho_{\text{eff}}(\omega)$, we define a broader (more rectangular) distribution, the

Fermi-Dirac like distribution.

$$
\varrho_{cp}^{(\text{fd})}(\omega) = A \cdot \left(\left\{ \begin{array}{l} \dfrac{1}{e^{-\beta\left(\omega - \left(\omega_{cp}^{(-)} - \frac{1}{2}\Delta_{cp}^{(\text{fd})}\right)\right)} + 1}, \text{ for } \omega \leq \omega_{cp}^{(-)} \\[4ex] \dfrac{1}{e^{\beta\left(\omega - \left(\omega_{cp}^{(-)} + \frac{1}{2}\Delta_{cp}^{(\text{fd})}\right)\right)} + 1}, \text{ for } \omega > \omega_{cp}^{(-)} \end{array} \right. \right.
$$
$$
\left. + \left\{ \begin{array}{l} \dfrac{1}{e^{-\beta\left(\omega - \left(\omega_{cp}^{(+)} - \frac{1}{2}\Delta_{cp}^{(\text{fd})}\right)\right)} + 1}, \text{ for } \omega \leq \omega_{cp}^{(+)} \\[4ex] \dfrac{1}{e^{\beta\left(\omega - \left(\omega_{cp}^{(+)} + \frac{1}{2}\Delta_{cp}^{(\text{fd})}\right)\right)} + 1}, \text{ for } \omega > \omega_{cp}^{(+)} \end{array} \right. \right) \tag{48}
$$

The normalization factor A is, like above, not important for our considerations because we normalize eq. (48) like eq. (47) to fulfill the cavity protection condition (43a). $\Delta_{cp}^{(\text{fd})}$ is FWHM of the Fermi-Dirac-like cavity protection distribution and is, again, calculated numerically out of the boundary conditions (44). β describes the strength of how $\varrho_{cp}^{(\text{fd})}(\omega)$ rises/drops near $\omega_{cp}^{(\pm)} \mp \frac{1}{2}\Delta_{cp}^{(\text{fd})}$. For a big enough β, the two distributions will drop fast enough against zero so they won't overlap significantly.

Bibliography

[1] Y.Kaluzny, P.Goy, M.Gross, J.M.Raimond, and S.Haroche. Observation of self-induced rabi oscillations in two-level atoms excited inside a resonant cavity: The ringing regime of superradiance. *PHYSICAL REVIEW LETTERS 51, 1175*, 1983.

[2] J.H.Wesenberg, A.Ardavan, G.A.D.Briggs, J.J.L.Morton, R.J.Schoelkopf, D.I.Schuster, and K.Molmer. Quantum computing with an electron spin ensemble. *PHYSICAL REVIEW LETTERS 103, 070502*, 2009.

[3] R.H.Dicke. Coherence in spontaneous radiation processes. *PHYSICAL REVIEW 93, 99*, 1954.

[4] Y.Kubo, I.Diniz, A.Dewes, V.Jacques, A.Dreau, J.F.Roch, A.Auffeves, D.Vion, D.Esteve, and P. Bertet. Storage and retrieval of a microwave field in a spin ensemble. *PHYSICAL REVIEW A 85, 012333*, 2012.

[5] K.Henschel, J.Majer, J.Schmiedmayer, and H.Ritsch. Cavity qed with an ultracold ensemble on a chip: Prospects for strong magnetic coupling at finite temperatures. *PHYSICAL REVIEW A 82, 033810*, 2010.

[6] R.Amsuess, Ch.Koller, T.Noebauer, S.Putz, S.Rotter, and K.Sander. Cavity qed with magnetically coupled collective spin states. *PHYSICAL REVIEW LETTERS 107,060502*, 2011.

[7] A.Imamoglu. Cavity qed based on collective magnetic dipole coupling: Spin ensembles as hybrid two-level systems. *PHYSICAL REVIEW LETTERS 102, 083602*, 2009.

[8] K.Sandner, H.Ritsch, R.Amsuess, Ch.Koller, T.Noebauer, S.Putz, J.Schmiedmayer, and J.Majer. Strong magnetic coupling of an inhomogeneous nitrogen-vacancy ensemble to a cavity. *PHYSICAL REVIEW A 85, 053806*, 2012.

[9] I.Diniz, S.Portolan, R.Ferreira, J. M.Gerard, P.Bertet, , and A.Auffeves. Strongly coupling a cavity to inhomogeneous ensembles of emitters: Potential for long-lived solid-state quantum memories. *PHYSICAL REVIEW A 84, 063810*, 2011.

[10] D.Krimer. Solutions of the volterra integral equation for the different values of the probe frequency ω_p. Private communication, 2012.

[11] C.Gerry and P.Knight. *Introductory quantum optics*. Cambridge University Press, 2005.

[12] C.W.Gardiner and M.J.Collett. Input and output in damped quantum systems: Quantum stochastic differential equations and the master equation. *PHYSICAL REVIEW A 31, 3761*, 1985.

[13] R.Amsuess. Cavity input-ouptut formalism. Private communication, 2012.

[14] Florian Marquardt. Lecture quantum-optical phenomena in nanophysics. University Lecture, 2010.